ACS Catalysis

pubs.acs.org/acscatalysis Review

Dynamic Evolution of Zeolite Framework and Metal-Zeolite Interface

Zhong-Pan Hu, Jingfeng Han, Yingxu Wei,* and Zhongmin Liu*

Cite This: ACS Catal. 2022, 12, 5060−5076 Read Online

ABSTRACT: Zeolites and metal-zeolites are a class of porous materials that have been widely utilized in industry. So far, several fundamental questions relating to the dynamic evolution of the zeolite framework and the metal-zeolite interface remain unanswered. Contrary to the classical view of zeolites as a static, rigid, and changeless material, the framework atoms and foreign metals in zeolites can dynamically interconvert under the pretreatment or reaction conditions, making it difficult to identify the real active centers and mechanisms. With the development of characterization techniques and theoretical calculations, a more profound understanding of the dynamic evolution of zeolite framework and metal-zeolite interface at the atomic scale has been achieved. This critical Review will feature the recent progress of the dynamic evolution of zeolite and metal-zeolites, mainly focusing on the T−O−T bonds breaking and formation, metal valence state transformation, phase evolution, and migration. We compare these proposed mechanisms and analyze their suitability in distinct experimental conditions. We highlight that the identification of the active sites and catalytic mechanism of zeolites and metal-zeolites should be cautious and should consider the dynamic evolution of the active centers under reaction conditions. Finally, we summarize the usages and limitations of different characteristic techniques, propose some future research directions about the dynamic evolution of zeolites and metal-zeolites, and hope to bridge the gaps between the knowledge achieved in characterizations and the real nature of the active sites to guide zeolite-based materials synthesis, modification, and application.

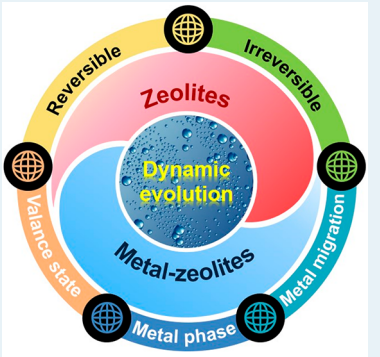

KEYWORDS: *zeolite, metal-zeolite, dynamic evolution, framework, interface, interconversion, heterogeneous catalysis*

1. INTRODUCTION

Catalysts are the footstone of the modern chemical industry, which can conspicuously accelerate the reaction rate, shorten the reaction time, and reduce energy consumption. As an important type of solid catalysts, zeolites have become the backbone in some crucial chemical processes, such as fluid catalytic cracking (FCC),[1,2] methanol-to-olefin (MTO),[3−6] methanol-to-ethanol,[7−9] and coupling conversion of hydrocarbon and methanol/CO_x to aromatization.[10−13] Zeolites are a class of crystalline microporous materials with a key feature of well-defined channels/cages for reactant molecules adsorption, transformation, and reaction, which are constructed from the connections of corner-sharing TO_4 tetrahedra (T = Si, Al, P, etc.). Owing to the presence of AlO_4 in aluminosilicate zeolites and SiO_4 in silicoaluminophosphate zeolites, the negative charge of zeolite framework requires a balancing cation (usually H^+) to ensure electroneutrality, resulting in another key feature of Brønsted acid sites (BAS).[14,15] By controlling the synthesis conditions, diverse metals (e.g., Ti, Sn, Ge, Zr, and Nb) can be introduced into the zeolite framework, forming heteroatomic zeolites with Lewis acidity.[16,17] Besides, the extra-framework metal species with single, cluster, and nanoparticle structures can be accommodated into zeolite channels/cages.[18−20] Until now, more than 250 topologies of zeolites with various compositions and acidities have been developed by bottom-up and top-down strategies, exhibiting many unrivalled catalytic performances (e.g., shape selectivity,[21−23] dynamic autocatalysis,[24,25] and synergistic catalysis).[26,27] Although a lot of progress has been achieved, many aspects of the active sites and catalytic mechanisms in zeolites and metal-zeolites are still under debate.

Ordinarily, zeolites are regarded as a rigid material owing to their high crystallinity, thermal stability, and renewability for various catalytic reactions. As a matter of fact, fast bond breaking and formation, metal valence state transformation, phase evolution, and migration can be observed over the zeolites and metal-zeolites even at a moderate temperature.[28−30] It is necessary to change the classical concept of zeolites as static and solid materials to a novel belief that to some extent, zeolites are dynamic, labile, and flexible under

Received: March 11, 2022
Revised: March 24, 2022
Published: April 14, 2022

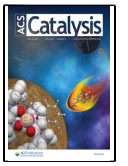

https://doi.org/10.1021/acscatal.2c01233
ACS Catal. 2022, 12, 5060−5076

practical reaction conditions. In general, the evolution of framework atoms and foreign metals in zeolites is strongly dependent on the reaction conditions (e.g., temperature, pressure, and steam/reductive/oxidative/acid/base atmosphere) and nature of zeolites (e.g., topology, Si/Al ratio, and crystallinity).[31,32] Representatively, H_2O can prolong the lifespan of SAPO-34 in MTO by depressing the coke formation or converting coke to active intermediates in MTO catalysts through decreasing the barrier for hydrogenation of heavy aromatic deposits to active aromatic intermediates[33,34] but can also cause zeolite dealumination, desilication, and deactivation.[35,36] Indeed, the metastable property of zeolites was found when they were first synthesized, but it has not been well understood in the past. With the development of *in situ* and operando characterization techniques and theoretical calculations, a lot of fundamental and in-depth understandings about the dynamic evolution of zeolites and metal-zeolites have been obtained, providing some useful directions and principles to synthesize and modify zeolite-based materials with optimal properties for target reactions.

This Review summarizes the recent processes of the dynamic evolution of zeolite framework and metal-zeolite interface under pretreatment or reaction conditions, aiming to bridge the gap between the measured and actual active sites. The interactions between the host zeolites/metal-zeolites and guest molecules will be globally and dynamically illustrated at the atomic level. The structure of this review is as follows: Section 2 presents the dynamic evolution of the zeolite framework, focusing on the T−O−T reversible and irreversible breaking and formation. The evolution mechanism of zeolites including aluminosilicates, aluminophosphates, and heteroatom zeolites will be compared and discussed. Section 3 reviews the dynamic evolution of metal species in metal-zeolites, mainly about the valence state transformation, phase evolution, and migration under reaction conditions. The mechanisms, characterizations, and novel findings will be summarized and discussed. In section 4, the challenges and outlook of the future research directions about the dynamic evolution of the active sites embedded into zeolites will be proposed and concluded.

2. DYNAMIC EVOLUTION OF ZEOLITE FRAMEWORK

Different from the classical concept of zeolite as a static material, the T−O−T bonds of zeolites can dynamically break and form under reaction conditions. Among the various studies, the interactions between zeolites and H_2O have drawn particular attention because H_2O is a common medium for zeolite synthesis, modification, and applications. It is known that H_2O is involved in the hydrolysis, condensation, and crystallization processes of zeolites but can also lead to zeolite destruction and deactivation. Therefore, making clear the interaction mechanisms is of great importance. However, these interactions are complex because the H_2O inside zeolites possesses distinct structures as compared with those in an environment without confinement.[37−41] Furthermore, the conditions (e.g., temperature, partial pressure, and amount) can affect the structure of H_2O (i.e., single, cluster, and bulk).[42−44] In this part, we clarify the dynamic evolution of zeolites into reversible and irreversible hydrolysis of T−O−T bonds and compare these mechanisms at the atomic level.

2.1. Reversible Breaking and Formation of T−O−T Bonds. *Aluminosilicate Zeolites.* Contrary to the classical view of zeolite as a static, rigid, and changeless material, recent studies found that the T−O−T bonds of zeolites could be reversibly broken and formed under moderate steam treatment conditions, showing a dynamic and reversible feature. For instance, Heard et al. developed a ^{17}O isotope labeling experiment using $H_2{}^{17}O$ and demonstrated that the CHA zeolite could be reversibly hydrolyzed in neutral liquid water without framework degradation.[28] They proposed a novel mechanism for Si−O bonds hydrolysis, in which the Si−O bonds started to be hydrolyzed through the interaction between a H_2O molecule and framework O. Subsequently, a H_2O molecules chain was formed and attached to the adjacent framework O, resulting in Si−O cleavage with a low barrier of 63 kJ mol^{-1}.[45,46] Ab initio molecular dynamic (AIMD) results revealed the Al−O bond hydrolysis was much easier than Si−O bonds so that the Al−O bonds could be hydrolyzed by a single H_2O to form a H_2OAlO_3 tetrahedron. Furthermore, ^{17}O isotope labeling experiments were performed, and the corresponding ^{17}O nuclear magnetic resonance (NMR) spectra exhibited obvious framework ^{17}O signals (Si-^{17}O-Si at 33 ppm and Si-^{17}O-Al at 20−25 ppm), demonstrating the presence of a quick equilibrium of hydrolyzed and unhydrolyzed zeolite framework in $H_2{}^{17}O$. This work gives a novel insight into the static zeolites that are labile and dynamic with fast bond breakage and recovery in H_2O atmosphere.

Later, Ashbrook and co-workers compared two zeolites (MOR and FER) and two agents ($^{17}O_2$ and $H_2{}^{17}O$), finding that the ^{17}O in these two zeolites were more easily enriched by $H_2{}^{17}O$ than $^{17}O_2$.[29] They also found that the ^{17}O-exchanged orders of different T−O−T bonds were strongly dependent on the type of guest molecules. In the atmosphere of $H_2{}^{17}O$, ^{17}O atoms preferentially incorporated into the Si−O−Al bonds, e.g., (Si−^{17}O−Al):(Si−^{17}O−Si) ratio of ∼1.3:1 for the MOR zeolite exchanged by $H_2{}^{17}O$ for ∼18 h. However, a (Si−^{17}O−Al):(Si−^{17}O−Si) ratio of ∼0.18:1 was obtained over the $^{17}O_2$-exchanged MOR zeolite at the same condition, which is similar to the calculated (Si−O−Al):(Si−O−Si) ratio (∼0.2:1, Si/Al = 11). Besides, they investigated the ^{17}O-exchanged behavior of Na-MOR in $H_2{}^{17}O$ and found that the enrichment of ^{17}O in Na-MOR was slower than H-MOR zeolite, suggesting the Na^+ had negative effects on the isotopic exchange process. However, the mechanisms were not proposed and confirmed. Recently, Sholl and co-workers studied the hydrolysis mechanisms of the first Al−O bond in protonic and cationic (Na, K, and Ca) LTA zeolites and demonstrated that the cationic LTA zeolites were more kinetically stable than H-LTA owing to the different dissociation processes of H_2O in H-LTA and cationic LTA zeolites.[47] Density functional theory (DFT) calculations revealed that the hydrolysis reaction in H-LTA followed the H_2O dissociation and proton transfer and rotation, while a second transfer of the proton was observed in cationic LTA zeolites. Therefore, the first Al−O bonds did not break concurrently with H_2O dissociation in cationic LTA zeolites, resulting in a higher energy barrier than that on H-LTA. Noticeably, the free energy for the Al−O−Si bond cleavage by two H_2O molecules is a little higher than that by a single H_2O molecule, which is different from some previous studies.[28,29] Therefore, more systematic and quantitative experiments are necessary to give more convincing evidence about the T−O−T breakage and formation mechanism of cationic zeolites.

Silicoaluminophosphate (SAPO) Zeolites. At nearly the same time as the above work was published, our work investigated the hydrothermal treatment of the aluminosilicate phosphate zeolites (SAPO-34) in $H_2{}^{17}O$ atmosphere, in which

https://doi.org/10.1021/acscatal.2c01233
ACS Catal. 2022, 12, 5060−5076

the dynamic and reversible breaking and formation of T−O−T bonds in SAPO-34 occurred at the moderate temperature in the range of 100−300 °C (Figure 1).[48] On the basis of ^{17}O

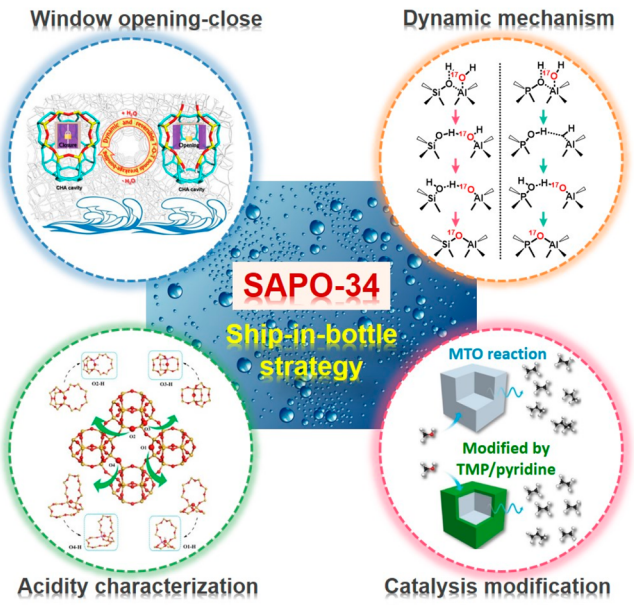

Figure 1. Ship-in-a-bottle strategy for acidity characterization and SAPO-34 catalyst modification for MTO reaction. Adapted with permission from ref 48. Copyright 2020 Wiley-VCH GmbH.

NMR spectroscopy, the dynamic incorporation of ^{17}O from $H_2{}^{17}O$ into the SAPO-34 framework were illustrated in detail. The 1D and 2D ^{17}O NMR spectra of the 300 °C-treated SAPO-34 in $H_2{}^{17}O$ possessed two obvious signals at around 21 ppm (Si-^{17}O-Al) and 48 ppm (P-^{17}O-Al), indicating the ^{17}O atoms were well incorporated into the SAPO-34 framework without obvious degradation. Owing to the relatively high $H_2{}^{17}O$-exchanged temperature, the ^{17}O incorporation mechanism was proposed: (i) A single H_2O was adsorbed onto Al atoms in both Si−O−Al and P−O−Al bonds. (ii) The T−O−T bonds were hydrolyzed through the formation of $SiO_3OH\cdots HOAlO_3$ and $PO_3OH\cdots HOAlO_3$. (iii) A dehydration reaction over $SiO_3OH\cdots HOAlO_3$ and $PO_3OH\cdots HOAlO_3$ resulted in the recovery of Si−O−Al and P−O−Al bonds.

Creatively, we took advantage of the reversible evolution of the T−O−T bonds in SAPO-34 zeolite to characterize the acidity of SAPO-34 through cointroduction of H_2O and trimethylphosphine (TMP)/pyridine. Multiple characterizations (^{1}H decoupled ^{31}P MAS NMR, ^{1}H MAS NMR, and confocal fluorescence microscopy measurements) demonstrated that a large amount of TMP and pyridine were introduced into the SAPO-34 cages with cofeeding H_2O and TMP/pyridine. However, almost no TMP/pyridine could be detected in SAPO-34 when only TMP/pyridine was introduced for adsorption and diffusion, demonstrating that the H_2O molecule could open the 8-membered ring (8-MR) window of SAPO-34. Furthermore, theoretical calculations confirmed that the diffusions of TMP and pyridine in the 8-MR window of SAPO-34 were not feasible with a high energy barrier of ∼40 kcal mol^{-1}. When one or two T−O−T bonds in the 8-MR window were broken, the diffusion energies for TMP and pyridine could be dramatically decreased, that is, 13.8 and 6.5 kcal mol^{-1} for TMP and pyridine diffusion through the 8-MR window of SAPO-34 with two opposite T−O−T bonds broken. The reversible breaking and formation of T−O−T bonds in SAPO-34 helped to realize the introduction of TMP and pyridine into the cavities of SAPO-34, which can be used to characterize the acidity of zeolites with smaller pore windows than probe molecules.

Another innovation, the TMP/pyridine modified SAPO-34 zeolites were applied for MTO reactions, exhibiting improved ethene selectivity. The pyridine accommodation established the diffusion obstacle for the produced long-chain alkenes, which improved the catalytic performance of SAPO-34 zeolite in the MTO reaction. This ship-in-a-bottle strategy is an effective way to illustrate the dynamic and reversible evolution of zeolite, to characterize the zeolite acidity, and to functionalize the zeolites for various applications including MTO. Very recently, a similar work about the dynamic evolution of the SAPO-34 framework in MTO was reported by Dai and co-workers that the hydrolysis of P−O−Al bonds was found in the spent SAPO-34 after a short time stream treatment at a high reaction temperature of ∼400 °C.[49] With the proceeding of MTO, hydrocarbon pool species would be formed in the cages and pores of SAPO-34, which could cover some BAS and P−O−Al bonds and thereby prevent the SAPO-34 framework from hydrolysis by H_2O. Contrast experiments about SAPO-34 with/without precoking illustrated that the organic deposits in SAPO-34 zeolite could act as a protective agent to enhance the stability of SAPO-34 zeolite.

Apart from H_2O, other guest molecules (e.g., methanol) can lead to the reversible evolution of the zeolite framework. Recently, Zheng and co-workers reported that the methanol adsorbed onto the pristine SAPO-34 zeolite could induce a frustrated Lewis pair (FLP, three-coordinated framework Al as Lewis acid site and SiO(H) as Lewis basic site), which was favorable for the formation of surface methoxy species (SMS) during MTO reaction.[50] Multiple characterizations and theoretical calculations revealed that the methoxy species were first bonded to the framework Al in the induced FLP state with the hydroxyl proton attached to the Lewis base sites, and the dynamic evolution of FLP could accelerate the catalytic reaction. *In situ* DRIFT experiments about $^{16}O/^{18}O$-methanol adsorption demonstrated that the oxygen species in SMS were from the methanol, confirming the proposed mechanism. This work gives a novel and dynamic insight into the active sites and catalytic mechanism of MTO reaction and proposes a possible route for SMS species formation. Later, Chen et al. extended the FLP concept into the supramolecular in MTO reaction using SAPO-34 and ssz-13 zeolite, in which the polymethylbenzenium (PMB^+) functioned as the Lewis acid to accept an electron pair, and the deprotonated framework oxygen site acted as the Lewis base to donate an electron pair.[51] Theoretical calculations and experimental results verified that this FLP could catalyze H_2 heterolysis and dehydrogenation of alkanes. This work convinces us that the identification of the active sites and catalytic mechanisms should be cautious and should consider the dynamic evolution of intermediates during the catalytic process.

Heteroatomic Zeolites. In the 1990s, several studies reported that the Si−O−Ti bonds in TS-1 zeolites could be reversibly transformed into the titanol Ti−OH and the silanol Si−OH species, and the Ti═O bonds could reversibly convert to $SiO_2Ti(OH)_2$.[52,53] Later, To et al. studied the interactions between H_2O and Ti sites using a hybrid quantum

https://doi.org/10.1021/acscatal.2c01233
ACS Catal. 2022, 12, 5060−5076

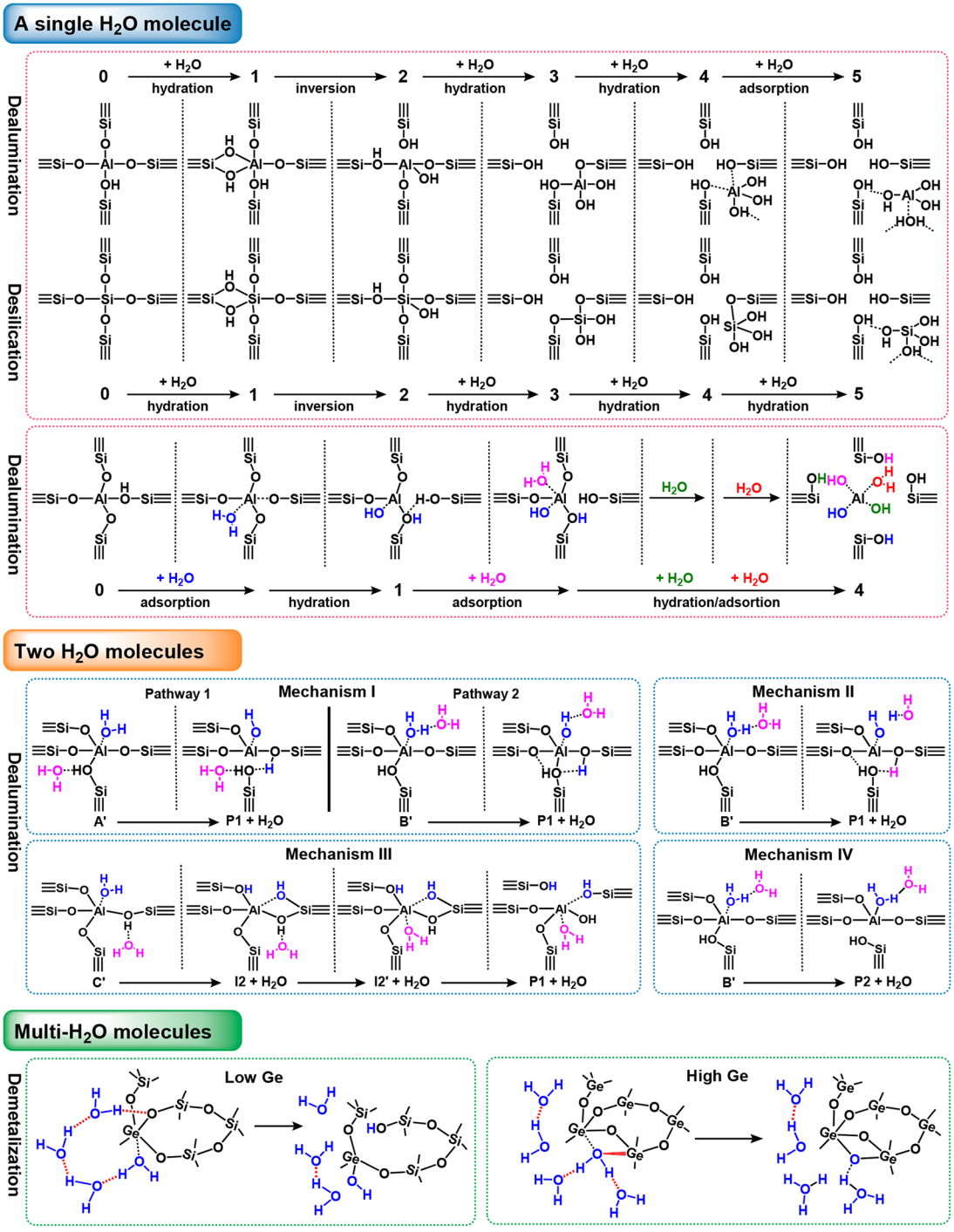

Figure 2. Proposed mechanisms for zeolite hydrolysis include a single H_2O molecule mechanism,[61,63] two H_2O molecules mechanism,[68] and multi-H_2O molecules mechanism.[82] Adapted with permission from refs 61, 63, 68, and 82. Copyright 2012 Wiley-VCH Verlag GmbH & Co. KGaA, Weinheim; Copyright 2015 American Chemical Society; and Copyright 2021 American Chemical Society.

mechanical/molecular mechanical method.[54] In the presence of one H_2O molecule, the insertion of one H_2O increased the coordination number of Ti atom from four to five in the tetrapodal, tripodal, bipodal, and titanyl configurations, and then from five to six. In the presence of two H_2O molecules, there are two models (i.e., mono(aquo) and bis(aquo) complexes). Particularly, bis(aquo) tripodal model was the most stable structure, suggesting that the hydrolysis and inversion of tetrahedral sites could boost the reactivity of Ti sites with H_2O. Furthermore, Qi et al. developed a two-dimensional proton-detected $^{1}H/^{119}Sn$ correlation solid-state NMR spectroscopy to characterize Sn-Beta zeolites before and after hydrolysis by H_2O, revealing the presence of reversible interconversion of Sn sites in Beta zeolites.[55] Typically, Sn-Beta zeolite with 97.4% ^{119}Sn was synthesized using isotope ^{119}Sn precursor. Then, two-dimensional ^{1}H $\{^{119}Sn\}$ HMQC MAS NMR experiments were performed over ^{119}Sn-Beta dehydrated at 393 K with and without ^{119}Sn decoupling. Similar to the monoalkyl-$SnCl_{3-x}(OH)_x$, the two-dimensional ^{1}H $\{^{119}Sn\}$ HMQC MAS NMR spectra of ^{119}Sn-Beta

https://doi.org/10.1021/acscatal.2c01233
ACS Catal. 2022, 12, 5060−5076

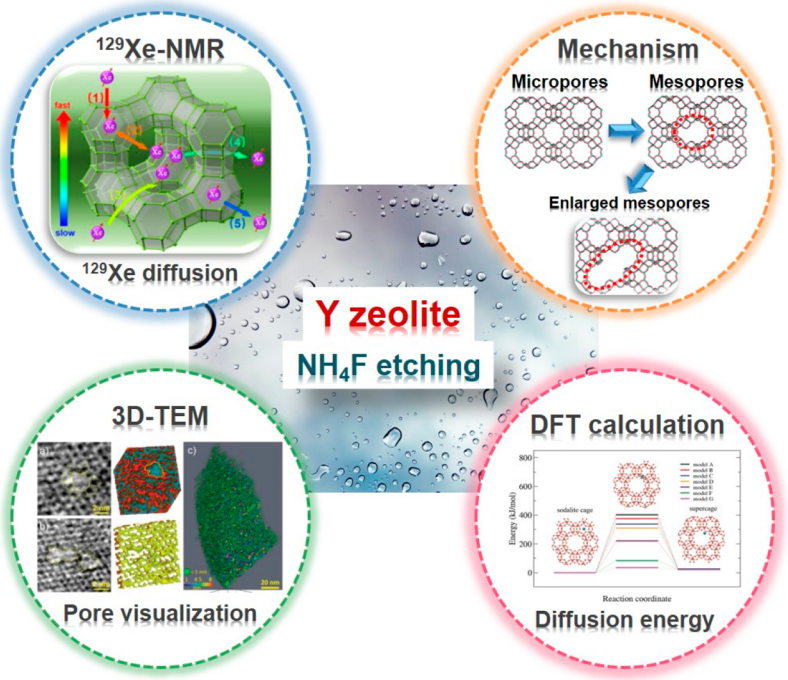

Figure 3. Dynamic evolution of Y zeolites from micropores to mesopores and enlarged mesopores characterized by 3D-TEM, Xe-NMR, and DFT calculations. Adapted with permission from ref 71. Copyright 2021 Wiley-VCH GmbH.

dehydrated at 393 K exhibited four signals, suggesting the presence of two types of open Sn sites ($(SiO)_3Sn-OH$) located at different T sites. Furthermore, ^1H $\{^{29}Si\}$ D-HMQC NMR experiments were conducted over ^{119}Sn-Beta dehydrated at 393 and 673 K, showing an obvious decrease of the signal of $Si(OSi)_3OH$, which was due to the transformation of open $(SiO)_3Sn-OH$ to closed $(SiO)_4Sn$ species. When the ^{119}Sn-Beta was rehydrated, the closed $(SiO)_4Sn$ could be transformed into $(SiO)_3Sn-OH$ species, showing a visible signal in the ^1H $\{^{119}Sn\}$ HMQC NMR spectrum. This work develops the approach of solid-state NMR spectroscopy to identify the dynamic and reversible interconversion of $(SiO)_3Sn-OH$ and $(SiO)_4Sn$ species in zeolites, giving an insight into the dynamic evolution of metal sites in heteroatomic zeolites.

2.2. Irreversible Breakage of T−O−T Bonds. The irreversible breakage of T−O−T bonds is a common phenomenon in zeolites, such as dealumination, desilication, and secondary pore formation, which would result in a partial loss in acidity, structure collapse, and/or zeolite deactivation.[56−58] Different from the reversible breakage of T−O−T bonds, the irreversible breakage of T−O−T bonds is a violent reaction, in which the framework T−O−T bonds would be deeply broken or even be removed from the framework. Herein, the irreversible breakage of T−O−T bonds over different zeolites are compared and discussed.

Aluminosilicate Zeolites. It is known that zeolites can be hydrolyzed in acidic and alkaline solutions.[59,60] However, these processes are difficult to control, usually leading to structure collapse and inhomogeneity demetalization from the surface to the interior of zeolites. As a neutral medium, H_2O vapor and steam can be used as a suitable agent to control the zeolite modification through adjusting the H_2O partial pressure and treatment temperature. However, the interactions between H_2O and zeolites are complex owing to the complex structure of H_2O molecules.

To simplify the interactions between H_2O and zeolites, Swang and co-workers chose a natural first strategy by adding H_2O molecules sequentially (Figure 2, a single H_2O molecule).[61] As a consequence, the demetalization processes can be regarded as a series of hydration reactions: (i) Dealumination process: First, hydration results in a vicinal disilanol defect, and reorientation of the vicinal disilanol creates a Si−OH and an Al−OH. Second, hydration produces two Si−OH and two Al−OH. Third, hydration results in $Al(OH)_3$ with hydrogen bond to Si−OH. Fourth, H_2O molecule adsorption generates the final $Al(OH)_3(H_2O)$ compound. (ii) Desilication process: Similar but different to the dealumination process, the fourth hydration results in $Si(OH)_4$ rather than $Al(OH)_3(H_2O)$. However, very high barriers for dealumination (190 kJ mol^{-1}) and desilication (260 kJ mol^{-1}) were obtained. Later, a microkinetic model was built to analyze the dealumination process of H-SSZ-13 zeolite and found that the first hydrolysis step was insignificant for the kinetics of zeolite dealumination, and the fourth hydrolysis step could be used to estimate the dealumination rate at the temperature over 700 K.[62] Furthermore, several different mechanisms have been proposed for the Al−O bond hydrolysis. For instance, a Brønsted−Evans−Polanyi relationship was established by Silaghi et al. (Figure 2, a single H_2O molecule) that the H_2O adsorption on the Al atom at the antiposition to the Brønsted acid site to create a penta- or distorted tetra-coordinated Al species; subsequently, the adsorbed H_2O was dissociated at the adjacent framework O atoms, leading to the first Al−O(H) bond breaking with relatively low activation energies of ∼76−125 kJ mol^{-1}.[63,64] Very recently, a similar dealumination mechanism of H-BEA zeolite was proposed by Mei and co-workers using AIMD simulations.[65] It was found that the hydrolysis step started by proton transfer, and then one H_2O molecule attracted the Al atom at the antiposition of the protonated O_{Al} atom, resulting in one Al−O_{Al} bond breaking and one Al−O_W bond formation.

https://doi.org/10.1021/acscatal.2c01233
ACS Catal. 2022, 12, 5060−5076

The free energy barriers of these four hydrolysis steps are 16.6, 20.8, 69.3, and 50.0 kJ/mol, respectively, which are a little lower than those in MOR, FAU, and CHA zeolite. Recently, the distorted tetra-coordinated Al species were detected by Chen et al. using NMR at 35.2 T,[66,67] further confirming the possibility of the Brønsted−Evans−Polanyi relationship mechanism for T−O−T bond breakage.

In recent years, several studies proposed that the collective mechanism considering the interactions between H_2O molecules was more suitable for T−O−T bond irreversible breaking than a single H_2O mechanism.[68,69] For instance, Stanciakova et al. reported that the Al−O(H) scission was induced by two adsorbed H_2O molecules involving five mechanisms (Figure 2, two H_2O molecules):[68] (i) Mechanism I is identical to the previous reported single H_2O molecule model.[63,64] (ii) Mechanism II (water-mediated proton transfer) is similar to the mechanism I, but it only has dually coordinated mode B' which allows proton transfer and thereby lowers the reaction barrier. (iii) In mechanism III (water insertion), one H_2O would be adsorbed onto the original protonated oxygen atom and another H_2O would be attached on the Al atom, forming a vicinal disilanol with one H_2O adsorbed onto the original protonated oxygen atom; subsequently, Al−OH and Si−OH are formed after Al−OH-Si cleavage. (iv) In mechanism IV (spontaneous Al−O(H) breaking), Al−O(H) bond breaking occurs from a dually coordinated mode B'. By comparing these four mechanisms to the single H_2O mechanism, it was found that the second H_2O molecule could accelerate the Al−O(H) bond breaking, lowering the energy barriers. In fact, H_2O clusters with different structures (1D or 3D chain of H_2O molecules containing hydrogen bonds) could be formed in zeolites.[28,37,70] These H_2O molecules can collectively break the T−O−T bonds with a low activation barrier. In section 2.1, collective mechanisms about reversible breaking of T−O−T bonds and formation have been discussed in detail.

Apart from H_2O, several other reagents have been used for zeolite demetalization at the atomic level (e.g., $SiCl_4$ and NH_4F). A recent work by Mintova and our group demonstrated that the application of NH_4F for zeolite treatment could selectively open the sodalite (SOD) cages of Y zeolites by removing the framework T atoms from SOD cages.[71] This work illustrated the dynamic evolution in porosity, micropores to mesopores, and enlarged mesopores in Y zeolite, by multicharacterizations and DFT calculations (Figure 3): Three-dimensional transmission electron microscopy (3D-TEM) revealed that mesopores were initially formed by etching the wall of cages. Subsequently, two or multiple mesopores would merge into enlarged mesopores. NMR characterization about Xe diffusion demonstrated that Xe molecules were first penetrated through the opened SOD cages and then diffused to supercages of the mesoporous zeolites. DFT calculations confirmed that Xe diffusion between SOD and supercages likely took place at the defects of six-member-ring separating these two types of cages, which was caused by the NH_4F treatment. This study opens up an efficient way to achieve zeolites with controlling mesopores, thus improving the catalytic performance in 1,3,5 tri-isopropylbenzene dealkylation and *n*-octane hydroconversion.

SAPO Zeolites. Different from aluminosilicate zeolites, SAPO zeolites possess different T−O−T bonds (e.g., P−O−Al bonds and $(AlO)_3Si$−OH-Al microstructure), which usually exhibit some unique properties relative to aluminosilicate zeolites. In the 1990s, H_2O adsorbed in SAPO-34 has been studied by experiments and ab initio simulations, revealing the presence of hydronium (H_3O^+), $H_5O_2^+$ dimers, and $H_3O^+(H_2O)_n$ clusters in SAPO-34.[72,73] However, the violent reaction mechanism between H_2O and the SAPO zeolite framework is rarely reported. Recently, several studies based on theoretical calculations have been performed to study the demetalization processes of SAPO zeolites. For instance, Fjermestad et al. reported that the demetalization processes of SSZ-13 and SAPO-34 zeolites were strongly dependent on the proton location, in which the SSZ-13 and SAPO-34 zeolites possessed the same mechanism for the first T−O−T bond hydrolysis but the different mechanisms for deep hydrolysis.[74] Typically, the first T−O−T bond hydrolysis in both SSZ-13 and SAPO-34 was through the formation of a vicinal disilanol defect (Al-$(OH)_2$-Si). For SAPO-34, after the first T−O−T bond cleavage, the proton was transferred to a nearby Si−O−Al to form a Si−OH and three Al−O−Si species (S2b-H_2O), while in SSZ-13, the proton was still bonded to an oxygen atom (Si−OH-Al) with one Si−OH, one Al−OH, and one Si−O−Al (Z2-H_2O). Later, they proposed two new pathways for SAPO-34 desilication involving stepwise hydrolyses of Si−O−Al bonds:[75] (i) A single H_2O molecule was coordinated to Al atom rather than to the proton, lowering the Si−O−Al bond breaking energy. (ii) Two H_2O molecules were adsorbed onto the acidic proton and Al atom, respectively, to break the T−O−T bonds. As compared with the H_2O molecule interacting with an acidic proton,[74] H_2O molecule coordinated to Al atom can lower the activation barrier of T−O−T scission, which is crucial for the breakage of the T−O−T bonds. Furthermore, the formation of Si islands in SAPO-34 has been reported that the silanol nests generated by desilication could be healed by an available H_3PO_4 molecule, and the framework position of the P atom could be healed by the extra-framework $Si(OH)_4$.[76] Hence, Si islands were formed because of the repeated migration and location of framework and extra-framework P and Si species.

Furthermore, several experimental studies were carried out to illustrate the interactions between H_2O and SAPO zeolites. A typical example by Kolokathis et al. studied the instability of SAPO-37 after H_2O adsorption at different temperatures by *in situ* synchrotron radiation powder X-ray diffraction (SR-PXRD) and Fourier transform infrared spectroscopy (FTIR).[77] The *in situ* SR-PXRD and H_2O adsorption measurements revealed that the temperature could significantly affect the H_2O affinity and stability of SAPO-37: At the temperature below 345 K, SAPO-37 had the strongest affinity to H_2O, which could adsorb an order of magnitude more H_2O molecules than at the temperature above 345 K. As a consequence, the massive adsorbed H_2O in SOD cages could dramatically change the T−O−T angles of 4-rings at the SOD-d6r-SOD interface (e.g., the T−O_4−T angle decreased from 166° to 101° after it adsorbed H_2O in a matter of seconds), leading to the structure collapses. Therefore, the high concentration of H_2O around the acid centers and defects, together with the geometry of the framework, is the main reason for the structural destabilization of SAPO-37. Until now, only several experimental studies have been exploited to study the stability of SAPOs in hydrothermal treatment, which is probably due to the too rapid change of the structure to be directly evidenced.

Heteroatomic Zeolites. Previous publications have reported the interactions between H_2O molecules and heteroatomic

https://doi.org/10.1021/acscatal.2c01233
ACS Catal. 2022, 12, 5060−5076

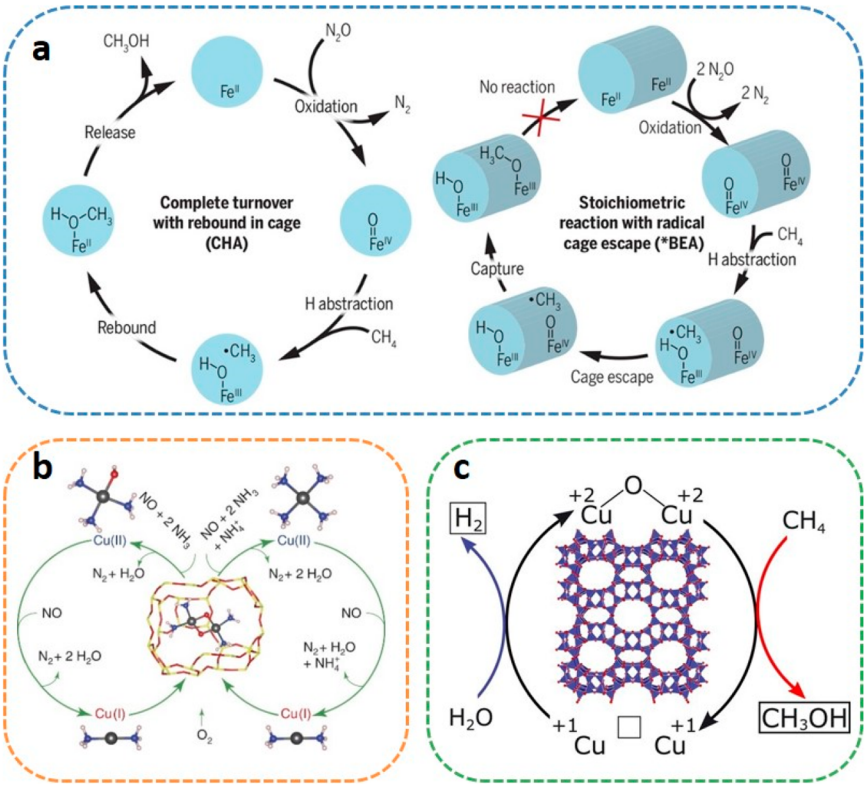

Figure 4. Valence state transformation of metal sites inside zeolites during the catalytic process: (a) the transformation of α-Fe(IV)═O in *BEA and CHA during methane hydroxylation.[95] (b) NH_3−SCR reaction mechanism of Cu-CHA.[107] (c) Selective anaerobic oxidation of methane to methanol over Cu-CHA by H_2O.[108] Adapted with permission from refs 95, 107, and 108. Copyright 2021 The American Association for the Advancement of Science and Copyright 2017 The American Association for the Advancement of Science.

zeolites (e.g., Sn-Beta, TS-1, and Ge-UTL).[78−82] Wolf et al. proposed two hydration pathways for Sn-Beta zeolites:[79] (i) A H_2O molecule in the second coordination sphere of Sn atom leads to the Sn−O−Si bond cleavage to a Si−OH and a Sn−OH. (ii) A H_2O molecule is coordinated to Sn atom and generates a Sn−(OH)−Si and a Sn−OH. Similar results were obtained by Sushkevich et al. that the H_2O could induce Brønsted acid sites in Sn-BEA zeolites.[80] By NMR and FTIR spectroscopy, they demonstrated the formation of new bridged OH groups (Sn-(OH)-Si) in Sn-Beta zeolite, which possessed strong Brønsted acidity and could lead to pyridine protonation. Besides, the type of guest molecules can affect the coordination states of Sn species. Yakimov et al. compared three different guest molecules (acetonitrile, methanol, and H_2O) adsorbed on Sn-Beta zeolites and found that the acetonitrile and methanol would be adsorbed on Sn atom to result in pentacoordinated Sn species, while a H_2O molecule was first adsorbed onto Sn to result in pentacoordinated Sn species and subsequently hexacoordinated species would be generated after long time reaction.[81]

Besides, the partial pressure of H_2O can affect the interactions between H_2O and zeolites. Jin et al. reported that the reversible and irreversible adsorption of H_2O on Ge-UTL zeolites was strongly dependent on the partial pressure of H_2O (Figure 2, multi-H_2O molecules).[82] H_2O sorption analysis indicated that the H_2O adsorption on Ge-UTL with different Si/Ge ratios was reversible at P/P_0 < 0.3 and irreversible at P/P_0 > 0.3. Mechanistic analysis based on molecular dynamics simulations suggested that the interactions between H_2O and Ge-UTL zeolite framework followed four mechanisms: (i) The equatorial-inversion mechanism for Ge-poor Ge-UTL in low H_2O partial pressure, a single H_2O molecular was attached to one Ge−O_f bond to form $Ge(O_fSi)_3O_wH$ (Q_3) and Si−O_fH. (ii) The vicinal mechanism for Ge-rich Ge-UTL in low H_2O partial pressure, a single H_2O was attached to two Ge−O_f bonds (Ge−O_f−Ge) to produce Ge-(O_fH_w)(O_wH_w)-Ge. (iii) The axial mechanism for Ge-poor Ge-UTL in high H_2O partial pressure, H_2O chain with four H_2O molecules (one-dimensional hydrogen bonds) was attached to Ge and the adjacent O atom in one Ge−O_f bond, resulting in Ge−O_wH and Si−O_fH species. (iv) S2R mechanism for Ge-rich Ge-UTL in high H_2O partial pressure, a H_2O molecule with two hydrogen bonds reacted with Ge atom to result in Ge-(O_f)(O_w)-Ge species and two protons in the channel, in which one of the protons tended to attach to the Ge-(O_f)(O_w)-Ge. In particular, the H_2O amount played a key role in determining the reversible and irreversible processes of Ge−O bonds: (i) Reversible breaking and formation of Ge−O bonds occurred in both Ge-poor and Ge-rich Ge-UTL zeolites in the condition of low H_2O partial pressure. (ii) In the presence of H_2O with high partial pressure, deep decomposition of Ge−O bonds would occur involving collective mechanisms (axial and S2R).

On the basis of the above analysis, it can be concluded that the guest molecules tend to coordinate to the metal sites in heteroatomic zeolites and weaken the M−O−Si bond by increasing the coordination number of metal sites which cause the cleavage of the M−O−Si to form M−OH and Si−OH bonds. However, most studies are focused on only one H_2O molecule or step-by-step hydrolysis process, which cannot

https://doi.org/10.1021/acscatal.2c01233
ACS Catal. 2022, 12, 5060−5076

reflect the real dynamic interactions between H_2O and metal sites. Furthermore, metal species in zeolites as heteroatoms only possess low amounts and LAS, which are hard to identify by some characterization techniques such as XRD, NMR, and FTIR spectroscopy. Therefore, more efficient characterization approaches should be developed to give more convincing evidence about the dynamic evolution of heteroatoms in the zeolite framework.

3. DYNAMIC EVOLUTION OF METAL SITES IN METAL-ZEOLITES

The introduction of metal species into zeolites is a promising and efficient approach to construct solid catalysts. The channels/cages of zeolites are smaller than 1 nm, which can provide a confined microenvironment to stabilize metal species and modify their chemical and electronic properties. Different from the framework atoms of zeolites, the metal species in zeolites possess various structures and states, which can interconvert to each other under different conditions. In recent years, the dynamic evolution of foreign metals in zeolites has been gradually discovered and illustrated. Herein, we summarize the recent progress about the dynamic evolution of metal sites in zeolites, mainly about the valence state transformation, metal phase transformation (metal carbides and metal hydrides), and metal migration.

3.1. Valence State Transformation. Supported metal species on zeolite generally possess several different states, which are strongly dependent on the loading amount, synthesis conditions, and support types. During the catalytic reaction, the valence states of metal species can be transformed from one to another, showing reversible and/or irreversible features.[83−85] Over the past several years, the dynamic evolution of metal active sites in zeolites have been found in several catalytic reactions (e.g., methane dehydroaromatization (MDA),[85] selective catalytic reduction (SCR) of nitrogen oxides (NO_x),[86,87] and methane oxidation to methanol).[83,88−91] In these reactions, the dynamic evolution of valence states of the supported metal species can induce the energetically feasible with lower activation energy. In the following subsection, a case-by-case discussion about the dynamic evolution of Fe and Cu species in zeolites will be provided in detail.

It is known that Fe species possess three typical valence states, i.e., +3, +2, and 0, which can be interconverted under different oxidative or reductive conditions ($Fe_2O_3 \leftrightarrow Fe_3O_4 \leftrightarrow FeO \leftrightarrow Fe$). Being confined in zeolites, the states of Fe species can be increased because the zeolite microenvironment can stabilize Fe sites with a high coordination number.[92−95] Consequently, the dynamic evolution of the unique structure of Fe species in zeolite would result in many special performances. A typical example by Snyder et al. reported that the Fe species confined by CHA and BEA zeolites exhibited different renewability in the reaction of CH_4 hydroxylation to CH_3OH due to the presence of different cages in CHA and BEA (Figure 4a).[95] From the topological structure perspective, the Fe-BEA and Fe-CHA zeolites possess high similarity in the first coordination spheres (mononuclear and high-spine Fe(IV)═O species) but different local porous environments (i.e., α-Fe(IV)═O in BEA and CHA can be accessed through 12-MR (5.9 Å) and 8-MR (3.7 Å), respectively). Therefore, the reactant CH_4 with van der Waals diameter of 4.1−4.2 Å diffuse through the pore aperture must be hindered in CHA (3.7 Å). After the C−H bond breaking, the CH_3 radicals formed in small pore CHA zeolite cannot be released from the active sites, accelerating CH_3 radicals to form CH_3OH rather than deactivated Fe−O−CH_3 species. As to Fe-BEA, CH_3 radicals can be easily released from the Fe active sites in BEA zeolite with large pore apertures, resulting in deactivated Fe species in the form of α-Fe(III)−OH and α-Fe(III)−OCH_3. Therefore, 40% of active sites in Fe-CHA can be regenerated during the CH_4 oxidation process, while Fe-BEA deactivates completely after a single turnover. Furthermore, the dynamic evolution of Fe states has been found in the supported dimeric Fe complexes toward CH_4 selective oxidation and NO_x-SCR.[96−99] Different from single Fe sites, there are several kinds of dimeric Fe species in zeolites, for example, 2 × $[FeO]^+$, $[OFe(\mu\text{-}O)Fe]^{2+}$, and $[Fe(\mu\text{-}O)_2Fe]^{2+}$.[96] A recent study about the CH_4 selective oxidation on Fe/ZSM-5 was reported in which the initial Fe sites ($[(H_2O)_2$−Fe(III)−$(\mu O)_2$−Fe(III)−$(H_2O)_2]^{2+}$) could be first oxidized by H_2O_2 to form Fe(III)-oxo and Fe(IV)-oxo complexes.[97] Then, the oxidized Fe sites promoted the C−H bond scission through three possible mechanisms: heterolytic, hemolytic methane dissociation, and Fenton-type reaction. Notably, the dynamic evolution of Fe sites gives rise to Fe(III)-oxo and Fe(IV)-oxo from $[(H_2O)_2$−Fe(III)−$(\mu O)_2$−Fe(III)−$(H_2O)_2]^{2+}$ species. These two Fe species working as the reaction centers significantly decreased the activation energy of C−H bond cleavage.

Zeolites with Cu confined ions are one of the most widely reported metal-zeolites for several reactions (e.g., NH_3−SCR and CH_4 oxidation to CH_3OH). Typically, Cu has +1 and +2 valence states and can reversibly transform from one to another, showing the oxidation−reduction property.[100−102] After the introduction of Cu species into zeolites, the framework O atoms can provide a 4-fold coordination environment to stabilize Cu ions, modifying the nature of Cu species. In the 1970s, Cu-exchanged Y zeolite was reported as an efficient catalyst for NH_3−SCR of NO_x, but the catalytic mechanism was not proposed and demonstrated.[103] In recent years, the type of Cu active sites in zeolites has been identified, for example, isolated Cu species ($ZCu^{2+}OH$, ZCu^+, and Z_2Cu^{2+}; Z represents zeolite) and dimeric Cu complexes (Cu^{2+}−O-Cu^{2+}).[104−106] These Cu active sites application in the NH_3−SCR reaction exhibit different activity, stability, and mechanism, in which the dynamic evolution of Cu ions in zeolite plays crucial roles in determining reaction performance and exact mechanistic pathways. For example, Paolucci et al. reported that isolated Z_2Cu^{2+} could travel through adjacent CHA zeolite windows to form transient Cu^{2+}−O−Cu^{2+} pairs during SCR reaction, providing a suitable configuration for O_2-mediated $Cu^+ \rightarrow Cu^{2+}$ redox step (Figure 4b).[107] It is worthwhile to note that the electrostatic tethering to framework Al sites and the limited volume of CHA zeolite cage can only result in one Cu^{2+}−O-Cu^{2+} pair. By the aid of steady-state measurements, characterizations, and theoretical calculations, the catalytic mechanisms on single Cu^{2+} and the Cu^{2+}−O−Cu^{2+} pair were determined as the following: single Cu^{2+} catalyzed the reduction, one SCR half-cycle, while Cu^{2+}−O−Cu^{2+} catalyzed the oxidation, the other SCR half-cycle. Accordingly, the reaction conditions and Cu density can significantly affect the dynamic evolution ability of Cu species, affecting the SCR performance of Cu-CHA catalysts. Apart from that, the dynamic evolution of Cu states in zeolite is also of great importance for methane selective oxidation to methanol.[108−112] Sushkevich et al. reported that Cu^{2+} centers

https://doi.org/10.1021/acscatal.2c01233
ACS Catal. 2022, 12, 5060−5076

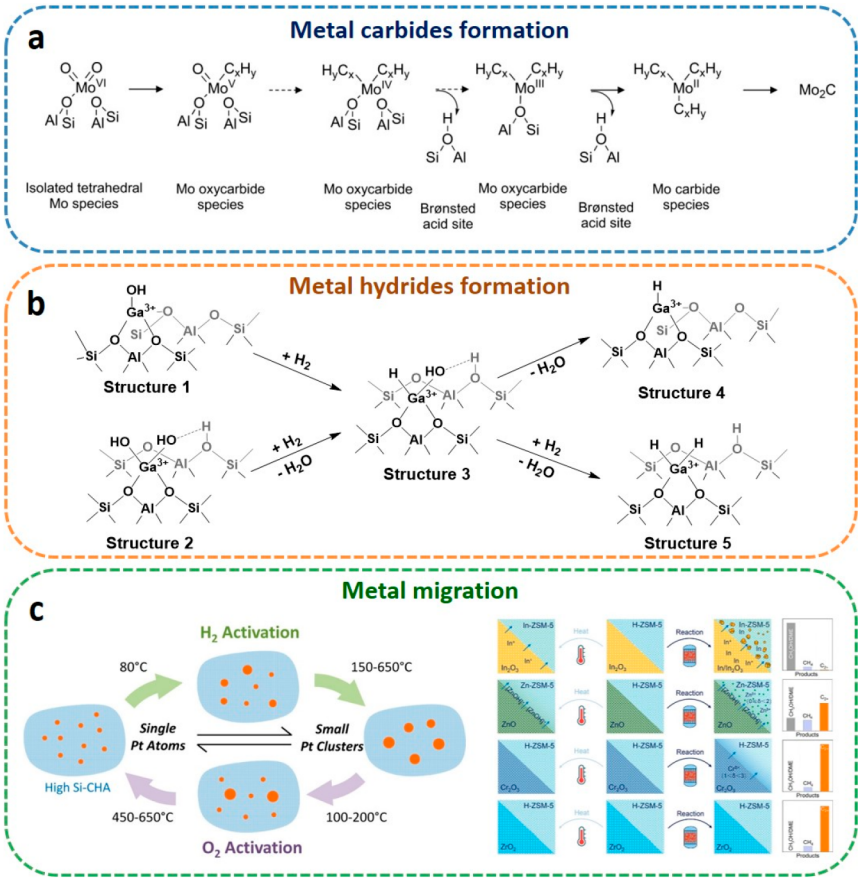

Figure 5. Dynamic evolution of foreign metals in zeolites during the catalytic process. (a) Schematic illustration of the dynamic evolution of Mo species in HZSM-5 during MDA reaction.[118] (b) Schematic illustration of the evolution of Ga species on MFI zeolites in H_2.[133] (c) Left, schematic illustration of transformation between single Pt atoms and small Pt clusters under different conditions;[146] Right, schematic illustration of the migration of In, Zn, Cr, and Zr on HZSM-5 during CO_2 hydrogenation reaction.[150] Adapted with permission from refs 118, 133, 146, and 150. Copyright 2016 Wiley-VCH Verlag GmbH & Co. KGaA, Copyright 2018 American Chemical Society, Copyright 2016 American Chemical Society, and Copyright 2021 Wiley-VCH GmbH.

would transform into Cu^+ during the beginning period of methane oxidation and then Cu^+ could be oxidized to Cu^{2+} by H_2O (Figure 4c).[108] Methanol desorption experiments, XAS and FTIR spectroscopic studies, and theoretical calculations illustrated that the reversible change of Cu ions ($Cu^{2+} \leftrightarrow Cu^+$) realized the regeneration of active centers, accelerated methanol desorption, and importantly minimized the activation energy of the selected pathway for methane to methanol. Different than O_2, the water returned two electrons, producing reactive Cu^{2+} and H_2. It is notable that only the limited size of CHA zeolite pores can generate mono(m-oxo)dicopper active sites, enabling H_2O acting as an oxidant to regenerate Cu sites and simultaneously stabilize reaction intermediates and transition states.

3.2. Metal Carbides. In many catalytic reactions (e.g., alkane conversion and Fischer−Tropsch synthesis) involving metal-zeolite catalysts, metal species existing in oxidation state in the fresh catalyst could transform into metal carbides during the reaction, thereby affecting the catalytic performance and mechanism.[83,85,113] Among the various metals, Mo and Fe species supported on HZSM-5 have been widely reported for the formation of metal oxycarbidic and carbide counterparts. In the fresh Mo-zeolite samples, there are many kinds of Mo species on zeolites, e.g., MoO_x cluster, isolated MoO_4 and MoO_6, MoO_4−MoO_6 chain, and MoO_3−O-MoO_3 dimer.[114] Upon utilization Mo-zeolite in MDA reaction, molybdenum oxycarbide (Mo_xC_yO), and carbide (Mo_xC_y) with different structures and stoichiometry would be formed with the reaction.[115−119] Recently, Lezcano-González et al. developed an operando XAS to study the nature of Mo species during MDA reaction and revealed that the dynamic evolution of Mo species inside HZSM-5 zeolites played key roles in determining the MDA performance (Figure 5a).[118] Initially, isolated Mo-oxo species would convert to MoC_xO_y species by CH_4, which were primarily responsible for C_2H_x/C_3H_x formation. With the reaction progress, MoC_3 clusters would be generated, which were responsible for benzene formation. The further long-time reaction led to the transformation of MoC_3 to larger Mo_2C-like nanoparticles on the external surface of HZSM-5 zeolite, which was less active. Furthermore, CO-FTIR, dynamic nuclear polarization (DNP) measurements and DFT calculations confirmed the transformation of Mo species within zeolites.[119,120] To make full utilization of the dynamic evolution of Mo species, the chemical looping process is introduced into the Mo-zeolites catalyst system for MDA reaction, which can improve the activity and efficiency.[121,122] Apart from the Mo sites, iron carbide species have been reported in Fe-zeolite catalysts toward hydrocarbon transformation.[123−125] These findings can help us to better understand the actual active sites

https://doi.org/10.1021/acscatal.2c01233
ACS Catal. 2022, 12, 5060−5076

and catalytic mechanism of metal-zeolites in actual reaction conditions and guide meal-zeolites design and synthesis.

3.3. Metal Hydrides. Surface hydrides have been reported over the past several decades but are difficult to identify owing to their complexity and instability.[126,127] Zeolites possess a well-defined structure, which is beneficial to clarify the evolution process of metal to metal hydrides. In recent years, several studies reported that metal species inside zeolites could transform into metal hydrides, which could act as the active sites for various catalytic reactions, e.g., alkane dehydrogenation and hydrocarbon dehydroaromatization. For instance, there are many kinds of Ga species in the Ga-zeolites, such as Ga_xO_y, Ga^+, $[GaO]^+$, $[GaH_2]^+$, $[Ga(OH)_2]^+$, $[GaH(OH)]^+$, and $[GaH]^{2+}$.[128] Under the H_2 atmosphere at high temperature, the oxidized Ga species can be transformed to GaH_x.[129−135] *In situ* FTIR experiments demonstrated that the Ga species variation could replace the acidic proton sites (BAS) of zeolite and subsequently formed Ga monohydride and Ga dihydride during H_2 reduction.[129,130] Later, Bell and co-workers characterized the isolated Ga^{3+} cations in Ga/HZSM-5 zeolites under oxidizing and reducing conditions by XAS measurements, revealing the presence of $[Ga(OH)_2]^+$ or $[Ga(OH)_2]^+$-H^+ cation pairs in oxidizing conditions and $[Ga(OH)_2]^+$-H^+ cation pairs, $[GaH_2]^+$-H^+, and $[GaH]^{2+}$ in H_2 atomosphere.[133] Theoretical calculations demonstrated that the type of Ga species on Ga-zeolites was strongly dependent on the pretreatment conditions and the location (next-nearest neighbor (NNN) and next-next-nearest neighbor (NNNN) framework Al atoms) (Figure 5b): In the conditions of H_2O pressure of 10 Pa and H_2 partial pressure $<10^2$ Pa for all the temperatures, $[Ga(OH)_2]^+$-H^+ cation pairs in NNNN sites are the most stable structure. When the temperature was higher than 623 K, $[Ga(OH)_2]^+$-H^+ cation pairs in NNN sites would transform to $[Ga(OH)]^{2+}$. When the H_2 partial pressure is in the range of 10^3−10^5 Pa with 10 Pa H_2O, $[Ga(OH)_2]^+$-H^+ cation pairs in NNNN sites would undergo further hydrogenation to form $[Ga(OH)H]^+$−H^+ pairs. At the H_2 pressure of $>10^5$ Pa and temperature of >673 K, $[GaH_2]^+$−H^+ pairs would be formed from $[Ga(OH)H]^+$−H^+ pairs in NNNN sites. For Ga species at NNN sites, at temperature of <623 K and H_2 pressure of $>10^2$ Pa, $[Ga(OH)_2]^+$-H^+ cation pairs would convert to $[Ga(OH)H]^+$-H^+ pairs. When the temperature is higher than 623 K, these cations would transform to $[GaH_2]^+$ species. In different reactions and reaction periods, the various active sites of Ga-zeolites, for example, framework Ga species, tetrahedrally coordinated extra-framework Ga sites, and $[GaH_2]^+$, are demonstrated active for ethylene dehydroaromatization,[128,136] and GaH_x and Ga^+-H^+ pair sites are regarded as the active sites for alkane dehydrogenation.[131,132,134,135,137] Apart from GaH_x, InH_x and ZnH_x in zeolites have been also reported during pretreatment in H_2, which were proposed as the active sites for hydrocarbon transformation.[138−141]

3.4. Metal Migration. Metal leaching and sintering are inherent characteristics of supported metal catalysts, which would lead to catalyst deactivation during the catalytic reaction. Typically, the confinement of metal species within zeolites can improve the stability of metal sites. However, they still suffer from sintering at harsh reaction conditions, e.g., high temperature and reductive atmosphere. For a long time, the dynamic migration of metal species in zeolites has not been well understood owing to the complex structure of metal species and zeolites under practical reaction conditions. With the development of characterization techniques, great progress has been achieved over some metal-zeolites, e.g., Ag-MFI,[142] Pd/USY,[143,144] Pd-CHA,[145] Pt-CHA,[146] Pt-MCM-22,[147] PtSn@MFI,[148] Au/TS-1,[149] and metal oxides/HZSM-5.[150]

A typical example by Corma and co-workers reported that the Pt nanoparticles could be reversibly transformed to single atoms in high-silica CHA zeolite (Figure 5c, left).[146] By time-resolved X-ray absorption fine structure (XAFS) and *in situ* TEM techniques, the dynamic evolution of Pt species including the coordination environment and microtopography in CHA zeolites in different atmospheres and temperatures were obtained: Calcination in the air at 500 °C, Pt species with ∼3 Pt−O bonds at 2.01 Å and no Pt−Pt bonds could be observed in XAFS spectra, indicating the formation of isolated PtO_3 units within the CHA zeolites. When the oxidized Pt-CHA was treated in H_2 at the temperature of 25−400 °C, the Pt species would be gradually reduced to Pt clusters, as confirmed by a progressive decrease of the white line intensity at different temperatures. In particular, the onset temperature for Pt species reduction is lower than 100 °C, and the full reduction temperature is about 150 °C. After further oxidation of the reduced Pt-CHA, a progressive increase of the white line could be observed over the X-ray absorption near edge structure (XANES) spectra, suggesting the transformation of Pt−Pt bonds to Pt−O bonds. To further identify the local structure of Pt species, *in situ* high-angle annular dark field scanning transmission electron microscopy (HAADF-STEM) experiments were performed. A progressive disappearance of the Pt nanoparticles could be observed after exposure of the H_2-reduced Pt-CHA to O_2 at 500 °C, suggesting the redispersion of the Pt clusters to atomically Pt species. This study demonstrates that the Pt species in the types of single atoms and clusters can be tuned reversibly by controlling the calcination conditions, i.e., temperature and atmosphere. Furthermore, different pretreated conditions (i.e., CO + O_2, CO + H_2O, NO + CO, and NO + H_2) have been studied for Pt@MCM-22, showing similar trends to Pt-CHA.[147] Under reductive atmosphere (CO + O_2 and CO + H_2O), atomically dispersed Pt would aggregate into Pt clusters at the temperature of 100−300 °C. In an oxidative atmosphere (NO + CO and NO + H_2), Pt clusters would disperse into atomically Pt species at the temperature of 200−400 °C. These results suggest that the Pt species are strongly sensitive to the reactants and conditions. Therefore, the actual active sites of metal-zeolites should be globally and dynamically considered involving the reactant atmosphere and temperature.

Furthermore, the migration of metal oxides can be observed in oxide-zeolite system (metal oxide supported on zeolites). Recently, Wang and co-workers reported that the migration of metal oxides (In_2O_3, ZnO, Cr_2O_3, and ZrO_2) on HZSM-5 zeolite could be observed by HAADF-STEM, elemental mapping, and pyridine-FTIR techniques, which could affect the CO_2 hydrogenation performance (Figure 5c, right).[150] HAADF-STEM and elemental mapping revealed that the thermo-migration ability of metal species was strongly dependent on the metal species. A large amount of In and Zn species could be detected in HZSM-5 after CO_2 hydrogenation reaction, while almost no Cr and Zr species could be detected. Acidity characterizations (pyridine-FTIR and ammonia-temperature-programmed desorption (NH_3-TPD)) demonstrated that the In and Zn species could be easily migrated to the acidic proton sites of HZSM-5 via a solid ion-exchange mechanism, decreasing the acidity of HZSM-5.

https://doi.org/10.1021/acscatal.2c01233
ACS Catal. 2022, 12, 5060−5076

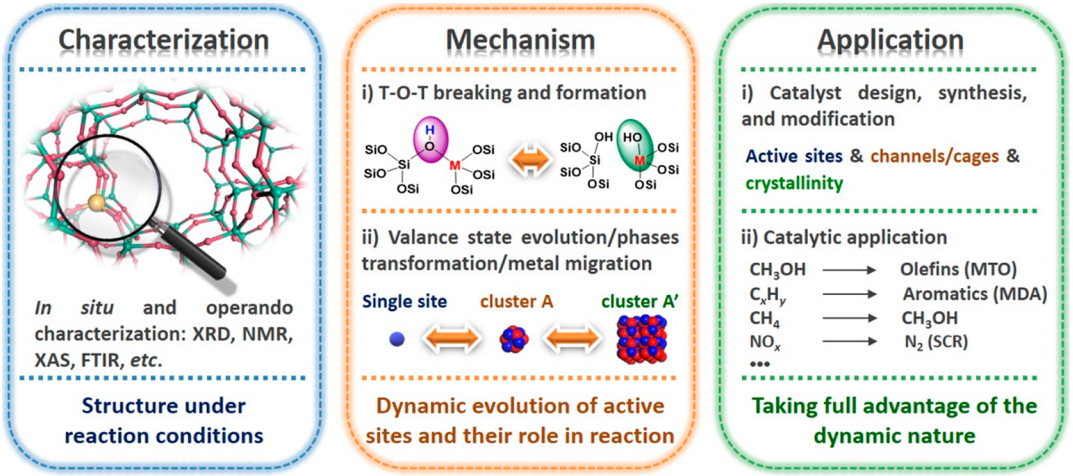

Figure 6. Future research directions about the dynamic evolution of zeolites and metal-zeolites.

Therefore, In_2O_3/HZSM-5 and ZnO/HZSM-5 exhibited much lower catalytic stability than Cr_2O_3/HZSM-5 and ZrO_2/HZSM-5 in CO_2 hydrogenation. The migration of metal oxides in zeolites is a common phenomenon for oxide-zeolites, but it is complex and has multiple pathways. Therefore, more systematic and quantitative experiments should be performed to determine the mechanism and driving force of the migration process of active metal species in zeolites.

4. CONCLUSION AND OUTLOOK

Herein, we review the dynamic evolution of the zeolite framework and metal-zeolite interface under various conditions (e.g., temperature, atmosphere, and partial pressure), uncovering some fundamental features about the active sites and catalytic mechanisms. We clarify the interactions between H_2O and zeolite framework and reveal the reversible and irreversible hydrothermal procedure. Further, we note that the number of H_2O molecules can significantly affect the T−O−T bond breaking and formation mechanisms. Furthermore, the type, composition, and topological structure of zeolites can affect the interactions between H_2O and zeolites and thereby affect the properties of zeolites. For metal-zeolites, the dynamic evolution of metal sites in zeolites is strongly dependent on the types of metal species and redox properties of the reactants. The evolution of valence states and migration of metals can be reversibly realized by controlling the oxidizing and reducing atmosphere. Besides, metal carbides and hydrides could be formed upon introducing hydrocarbons and hydrogen at a certain temperature. These controllable dynamical evolutions of the zeolite framework and metal-zeolite interface can be used as the approaches for zeolite modification and application. However, understandings about the dynamic evolution of framework and extra-framework atoms of zeolites are still scarce and far from complete and in-depth. It is necessary to exploit more experiments to make clear the dynamic evolution processes and synergetic effect of the framework and foreign metals including the location, dispersion mode, identification and evolution of active sites, and the formation and role of intermediates. In Figure 6, we propose three future research directions, including characterization, mechanism, and application.

4.1. Structure under Real Reaction Conditions. In the past, zeolites and metal-zeolites are usually characterized in static conditions. However, fast bond breaking and formation, evolution of metal valence states, phase transformation, and migration would occur over the zeolites and metal-zeolites during the catalytic reaction. Therefore, the identification of active sites and catalytic mechanisms should globally consider the evolution of zeolites and metal species under reaction conditions.

In recent years, many *in situ* and operando techniques have been exploited for the characterization of zeolite-based catalysts, which can give some credible information about the dynamic evolution of the zeolite framework and metal-zeolite interface. For instance, time-resolved Rietveld refinement of XRD and NMR have been used to reveal the type of Al species and the evolution of the zeolite crystallinity.[151−153] However, some zeolites and metal-zeolites contain only a small amount of metal species, which cannot be detected by XRD and NMR techniques. Therefore, more sensitive characterizations should be performed to distinguish these metal species. Recently, *in situ* XAS is used to characterize single metal atoms within zeolites, which can give information about the valence state, coordination number, and microstructure of framework and metal sites in zeolites, e.g., Al (three-coordinate, tetrahedral, and octahedral Al species),[154,155] Cu ($Cu^+ \leftrightarrow Cu^{2+}$),[108] and Mo ($Mo^{6+} \leftrightarrow MoO_xC_y \leftrightarrow Mo_2C$) species.[118] Also, 3D-TEM together with Xe-NMR have been used to study the dealumination process of faujasite (FAU) type zeolites, revealing the mesopore formation started by removing framework T atoms from sodalite cages.[71] However, the application of XAS and TEM techniques have some limitations, such as the difficulty in distinguishing the second core−shell atoms and light elements. *In situ* FTIR spectroscopy is used to monitor the evolution of hydroxy groups and probe molecules (e.g., pyridine, acetonitrile, and carbon monoxide) adsorbed onto zeolites, giving some important information about the structure and acidity of zeolites and metal-zeolites.[156,157] However, the interactions between H_2O and zeolites are hard to identify by FTIR because of the presence of complex hydrogen-bonding networks between Si−OH, Al−OH, and H_2O molecules. Besides, the FTIR experiments are usually performed at low temperature and diluted reaction atmosphere, which cannot reflect the nature of the active sites under reaction conditions. The development of more efficient

https://doi.org/10.1021/acscatal.2c01233
ACS Catal. 2022, 12, 5060−5076

and sensitive characterization techniques that are applicable at reaction conditions is very necessary. Apart from the *in situ* and operando approaches, the dynamic evolution process can be illustrated by rational design *ex situ* experiments, such as isotope labeling tests,[94,108,158] half-reactions with only one reactant,[108,159] and kinetic measurements.[160] Furthermore, theoretical calculations (i.e., AIMD) can be used to simulate the dynamic evolution of zeolite framework at picosecond scale.[50] Therefore, multiple techniques and theoretical calculations should be synchronously performed to identify the active sites and reveal the catalytic mechanism of zeolites and metal-zeolites.

4.2. Dynamic Mechanism of the Active Sites in Zeolites. Some dynamic procedures of framework atoms and foreign metals in zeolites are complex and very fast, which are difficult to be captured and identified. With the development of characterization techniques and theoretical calculations, some progress has been achieved step by step. Typically, the T−O−T bonds reversible/irreversible breaking and formation, demetalization mechanism, and the dynamic evolutions of foreign metals in zeolites have been illustrated in recent years. However, still many issues call for the solution (e.g., the precise location, number, kind, and structure of the framework atoms and foreign metals under reaction conditions). Furthermore, the complexity and variability of reaction mechanisms and pathways caused by the dynamic evolution of reaction active sites make research more challenging and require more advanced, sensitive, and dynamic techniques. Therefore, more efficient time-resolved and space-resolved approaches should be developed, and these advanced technologies should be applied to track the dynamic process of active centers and their catalytic roles in zeolite/metal-zeolite catalyzed reactions.

4.3. Taking Full Advantage of the Dynamic Nature of Zeolites and Metal-Zeolites. The hydrothermal process is crucial for both the construction of zeolite crystals and the converse process of degrading zeolite framework in a hydrothermal atmosphere for optimized distribution of acid sites and improved mass transfer. Over the past several years, H_2O vapor and steam have been used for zeolite modification (e.g., dealumination, desilication, and pore formation), improving the stability and diffusion properties of guest molecules. However, most studies are focused on the irreversible breaking of T−O−T bonds, mainly including zeolite destruction, collapse, and amorphization. The reversible evolution properties of zeolites are often overlooked. Recently, our work demonstrated that the reversible breaking and formation of T−O−T bonds of SAPO-34 could be used to introduce large molecules into small pore cages (ship-in-bottle strategy), thereby realizing acid sites recognition and MTO process adjusting.[48] These new strategies can be further promoted and applied. More creative, systematic, and reliable experiments and attempts are highly required to take full advantage of the dynamic evolution properties of zeolites in practical reactions.

For metal-zeolites, the dynamic evolution of metal species in zeolites has drawn particular attention in recent years, in which the varied active sites can accelerate the reactant activations or participate in the whole catalytic cycle. For example, the chemical looping process is introduced into some metal-zeolites (e.g., Mo/ZSM-5 and Fe-ZSM-5) for methane dehydroaromatization, which can improve activity and efficiency. In these processes, the Mo and Fe species can be dynamically interconverted from metal oxides to metal oxycarbidic and carbide counterparts. Owing to the participation of the lattice oxygen rather than oxygen molecule during the catalytic reaction, the energy consumption can be reduced. However, the metal-zeolites which are suitable for the operation mode of chemical looping process are limited, and the principles and mechanisms are still under debate.

In view of the current research of zeolite materials and catalysis, future studies are suggested to focus on the following aspects to realize some meaningful achievements: (i) developing *in situ*/operando spectroscopy techniques to make clear the dynamic nature of active sites and catalytic processes; (ii) making good use of the dynamic evolution property of zeolites and metal-zeolites for catalyst design, synthesis, modifications, and applications; and (iii) on the basis of the dynamic nature of catalytic materials and their roles in some important industrial process, developing dynamic modulation strategies to realize precise control and optimization of the zeolite materials and zeolite-catalyzed processes.

AUTHOR INFORMATION

Corresponding Authors

Yingxu Wei − *National Engineering Laboratory for Methanol to Olefins, Dalian National Laboratory for Clean Energy, iChEM (Collaborative Innovation Center of Chemistry for Energy Materials), Dalian Institute of Chemical Physics, Chinese Academy of Sciences, Dalian 116023, People's Republic of China;* orcid.org/0000-0002-0412-1980; Email: weiyx@dicp.ac.cn

Zhongmin Liu − *National Engineering Laboratory for Methanol to Olefins, Dalian National Laboratory for Clean Energy, iChEM (Collaborative Innovation Center of Chemistry for Energy Materials), Dalian Institute of Chemical Physics, Chinese Academy of Sciences, Dalian 116023, People's Republic of China; State Key Laboratory of Catalysis, Dalian Institute of Chemical Physics, Chinese Academy of Sciences, Dalian 116023, People's Republic of China; University of Chinese Academy of Sciences, Beijing 100049, People's Republic of China;* orcid.org/0000-0002-7999-2940; Email: liuzm@dicp.ac.cn

Authors

Zhong-Pan Hu − *National Engineering Laboratory for Methanol to Olefins, Dalian National Laboratory for Clean Energy, iChEM (Collaborative Innovation Center of Chemistry for Energy Materials), Dalian Institute of Chemical Physics, Chinese Academy of Sciences, Dalian 116023, People's Republic of China*

Jingfeng Han − *National Engineering Laboratory for Methanol to Olefins, Dalian National Laboratory for Clean Energy, iChEM (Collaborative Innovation Center of Chemistry for Energy Materials), Dalian Institute of Chemical Physics, Chinese Academy of Sciences, Dalian 116023, People's Republic of China*

Complete contact information is available at: https://pubs.acs.org/10.1021/acscatal.2c01233

Notes

The authors declare no competing financial interest.

ACKNOWLEDGMENTS

The authors are thankful for the financial support from the National Natural Science Foundation of China (Nos.

https://doi.org/10.1021/acscatal.2c01233
ACS Catal. 2022, 12, 5060−5076

22172166, 21991092 and 21991090), the Key Research Program of Frontier Sciences, CAS, Grant No. QYZDY-SSW-JSC024, the International Partnership Program of Chinese Academy of Sciences (121421KYSB20180007), the China Postdoctoral Science Foundation (2019M661147), the Excellent Postdoctoral Support Program of Dalian Institute of Chemical Physics, CAS, the Excellent Research Assistant Funding Project of CAS, and the Youth Innovation Promotion Association of CAS (No. 2021182).

REFERENCES

(1) Vogt, E. T. C.; Weckhuysen, B. M. Fluid Catalytic Cracking: Recent Developments on the Grand Old Lady of Zeolite Catalysis. *Chem. Soc. Rev.* **2015**, *44* (20), 7342−7370.
(2) Zhu, D.; Wang, L.; Fan, D.; Yan, N.; Huang, S.; Xu, S.; Guo, P.; Yang, M.; Zhang, J.; Tian, P.; Liu, Z. A Bottom-Up Strategy for the Synthesis of Highly Siliceous Faujasite-Type Zeolite. *Adv. Mater.* **2020**, *32*, No. 2000272.
(3) Tian, P.; Wei, Y.; Ye, M.; Liu, Z. Methanol to Olefins (MTO): From Fundamentals to Commercialization. *ACS Catal.* **2015**, *5*, 1922−1938.
(4) Ye, M.; Tian, P.; Liu, Z. DMTO: A Sustainable Methanol-to-Olefins Technology. *Engineering* **2021**, *7*, 17−21.
(5) Wu, X.; Xu, S.; Zhang, W.; Huang, J.; Li, J.; Yu, B.; Wei, Y.; Liu, Z. Direct Mechanism of the First Carbon-Carbon Bond Formation in the Methanol-to-Hydrocarbons Process. *Angew. Chem., Int. Ed.* **2017**, *56*, 9039−9043.
(6) Sun, T.; Chen, W.; Xu, S.; Zheng, A.; Wu, X.; Zeng, S.; Wang, N.; Meng, X.; Wei, Y.; Liu, Z. The First Carbon-carbon Bond Formation Mechanism in Methanol-to-hydrocarbons Process over Chabazite Zeolite. *Chem.* **2021**, *7*, 2415−2428.
(7) Cao, K.; Fan, D.; Li, L.; Fan, B.; Wang, L.; Zhu, D.; Wang, Q.; Tian, P.; Liu, Z. Insights into the Pyridine-Modified MOR Zeolite Catalysts for DME Carbonylation. *ACS Catal.* **2020**, *10*, 3372−3380.
(8) Gerald, O. Debut of a Coal-to-ethanol Plant. *Chem. Eng.* **2017**, *124*, 12.
(9) Liu, R.; Fan, B.; Zhang, W.; Wang, L.; Qi, L.; Wang, Y.; Xu, S.; Yu, Z.; Wei, Y.; Liu, Z. Increasing the Number of Aluminum Atoms in T_3 Sites of a Mordenite Zeolite by Low-Pressure $SiCl_4$ Treatment to Catalyze Dimethyl Ether Carbonylation. *Angew. Chem., Int. Ed.* **2022**, DOI: 10.1002/ange.202116990.
(10) Wei, C.; Yu, Q.; Li, J.; Liu, Z. Coupling Conversion of *n*-Hexane and CO over an HZSM-5 Zeolite: Tuning the H/C Balance and Achieving High Aromatic Selectivity. *ACS Catal.* **2020**, *10*, 4171−4180.
(11) Wei, C.; Li, J.; Yang, K.; Yu, Q.; Zeng, S.; Liu, Z. Aromatization Mechanism of Coupling reaction of Light Alkanes with CO over Acidic Zeolites: Cyclopentenones as Key Intermediates. *Chem. Catal* **2021**, *1*, 1273−1290.
(12) Chen, Z.; Ni, Y.; Zhi, Y.; Wen, F.; Zhou, Z.; Wei, Y.; Zhu, W.; Liu, Z. Coupling of Methanol and Carbon Monoxide over H-ZSM-5 to Form Aromatics. *Angew. Chem., Int. Ed.* **2018**, *57*, 12549−12553.
(13) Fang, X.; Liu, H.; Chen, Z.; Liu, Z.; Ding, X.; Ni, Y.; Zhu, W.; Liu, Z. Highly Enhanced Aromatics Selectivity by Coupling of Chloromethane and Carbon Monoxide over H-ZSM-5. *Angew. Chem., Int. Ed.* **2022**, DOI: 10.1002/anie.202114953.
(14) Zhong, J.; Han, J.; Wei, Y.; Tian, P.; Guo, X.; Song, C.; Liu, Z. Recent Advances of the Nano-hierarchical SAPO-34 in the Methanol-to-olefin (MTO) Reaction and Other Applications. *Catal. Sci. Technol.* **2017**, *7*, 4905−1923.
(15) Yang, M.; Fan, D.; Wei, Y.; Tian, P.; Liu, Z. Recent Progress in Methanol-to-Olefins (MTO) Catalysts. *Adv. Mater.* **2019**, *31*, No. 1902181.
(16) Shamzhy, M.; Opanasenko, M.; Concepcion, P.; Martinez, A. New Trends in Tailoring Active Sites in Zeolite-based Catalysts. *Chem. Soc. Rev.* **2019**, *48*, 1095−1149.
(17) Wang, N.; Sun, Q.; Yu, J. Ultrasmall Metal Nanoparticles Confined within Crystalline Nanoporous Materials: A Fascinating Class of Nanocatalysts. *Adv. Mater.* **2019**, *31*, No. 1803966.
(18) Chai, Y.; Wu, G.; Liu, X.; Ren, Y.; Dai, W.; Wang, C.; Xie, Z.; Guan, N.; Li, L. Acetylene-Selective Hydrogenation Catalyzed by Cationic Nickel Confined in Zeolite. *J. Am. Chem. Soc.* **2019**, *141*, 9920−9927.
(19) Zhong, J.; Han, J.; Wei, Y.; Xu, S.; He, Y.; Zheng, Y.; Ye, M.; Guo, X.; Song, C.; Liu, Z. Increasing the Selectivity to Ethylene in the MTO Reaction by Enhancing Diffusion Limitation in the Shell Layer of SAPO-34 Catalyst. *Chem. Commun.* **2018**, *54*, 3146−3149.
(20) Zhong, J.; Han, J.; Wei, Y.; Xu, S.; Sun, T.; Zeng, S.; Guo, X.; Song, C.; Liu, Z. Tuning the Product Selectivity of SAPO-18 Catalysts in MTO Reaction via Cavity Modification. *Chin. J. Catal.* **2019**, *40*, 477−485.
(21) Yang, M.; Li, B.; Gao, M.; Lin, S.; Wang, Y.; Xu, S.; Zhao, X.; Guo, P.; Wei, Y.; Ye, M.; Tian, P.; Liu, Z. High Propylene Selectivity in Methanol Conversion over a Small-Pore SAPO Molecular Sieve with Ultra-Small Cage. *ACS Catal.* **2020**, *10*, 3741−3749.
(22) Han, J.; Liu, Z.; Li, H.; Zhong, J.; Zhang, W.; Huang, J.; Zheng, A.; Wei, Y.; Liu, Z. Simultaneous Evaluation of Reaction and Diffusion over Molecular Sieves for Shape-Selective Catalysis. *ACS Catal.* **2020**, *10*, 8727−8735.
(23) Zhang, W.; Chen, J.; Xu, S.; Chu, Y.; Wei, Y.; Zhi, Y.; Huang, J.; Zheng, A.; Wu, X.; Meng, X.; Xiao, F.; Deng, F.; Liu, Z. Methanol to Olefins Reaction over Cavity-type Zeolite: Cavity Controls the Critical Intermediates and Product Selectivity. *ACS Catal.* **2018**, *8*, 10950−10963.
(24) Wu, X.; Xu, S.; Wei, Y.; Zhang, W.; Huang, J.; Xu, S.; He, Y.; Lin, S.; Sun, T.; Liu, Z. Evolution of C−C Bond Formation in the Methanol-to-Olefins Process: From Direct Coupling to Autocatalysis. *ACS Catal.* **2018**, *8*, 7356−7361.
(25) Lin, S.; Zhi, Y.; Chen, W.; Li, H.; Zhang, W.; Lou, C.; Wu, X.; Zeng, S.; Xu, S.; Xiao, J.; Zheng, A.; Wei, Y.; Liu, Z. Molecular Routes of Dynamic Autocatalysis for Methanol-to-Hydrocarbons Reaction. *J. Am. Chem. Soc.* **2021**, *143*, 12038−12052.
(26) Lin, L.; Sheveleva, A. M.; da Silva, I.; Parlett, C. M. A.; Tang, Z.; Liu, Y.; Fan, M.; Han, X.; Carter, J. H.; Tuna, F.; McInnes, E. J. L.; Cheng, Y.; Daemen, L. L.; Rudić, S.; Ramirez-Cuesta, A. J.; Tang, C. C.; Yang, S. Quantitative Production of Butenes from Biomass-derived γ-valerolactone Catalysed by Hetero-atomic MFI Zeolite. *Nat. Mater.* **2020**, *19*, 86−93.
(27) Gao, P.; Wang, Q.; Xu, J.; Qi, G.; Wang, C.; Zhou, X.; Zhao, X.; Feng, N.; Liu, X.; Deng, F. Brønsted/Lewis Acid Synergy in Methanol-to-Aromatics Conversion on Ga-Modified ZSM-5 Zeolites, As Studied by Solid-State NMR Spectroscopy. *ACS Catal.* **2018**, *8*, 69−74.
(28) Heard, C. J.; Grajciar, L.; Rice, C. M.; Pugh, S. M.; Nachtigall, P.; Ashbrook, S. E.; Morris, R. E. Fast Room Temperature Lability of Aluminosilicate Zeolites. *Nat. Commun.* **2019**, *10*, 4690.
(29) Pugh, S. M.; Wright, P. A.; Law, D. J.; Thompson, N.; Ashbrook, S. E. Facile, Room-Temperature ^{17}O Enrichment of Zeolite Frameworks Revealed by Solid-State NMR Spectroscopy. *J. Am. Chem. Soc.* **2020**, *142*, 900−906.
(30) Wouters, B. H.; Chen, T.-H.; Grobet, P. J. Reversible Tetrahedral-Octahedral Framework Aluminum Transformation in Zeolite Y. *J. Am. Chem. Soc.* **1998**, *120*, 11419−11425.
(31) Heard, C. J.; Grajciar, L.; Uhlik, F.; Shamzhy, M.; Opanasenko, M.; Cejka, J.; Nachtigall, P. Zeolite (In)Stability under Aqueous or Steaming Conditions. *Adv. Mater.* **2020**, *32*, No. 2003264.
(32) Simancas, R.; Chokkalingam, A.; Elangovan, S. P.; Liu, Z.; Sano, T.; Iyoki, K.; Wakihara, T.; Okubo, T. Recent Progress in the Improvement of Hydrothermal Stability of Zeolites. *Chem. Sci.* **2021**, *12*, 7677−7695.
(33) Zhao, X.; Li, J.; Tian, P.; Wang, L.; Li, X.; Lin, S.; Guo, X.; Liu, Z. Achieving a Superlong Lifetime in the Zeolite-Catalyzed MTO Reaction under High Pressure: Synergistic Effect of Hydrogen and Water. *ACS Catal.* **2019**, *9*, 3017−3025.

https://doi.org/10.1021/acscatal.2c01233
ACS Catal. 2022, 12, 5060−5076

(34) Zhou, J.; Gao, M.; Zhang, J.; Liu, W.; Zhang, T.; Li, H.; Xu, Z.; Ye, M.; Liu, Z. Directed Transforming of Coke to Active Intermediates in Methanol-to-olefins Catalyst to Boost Light Olefins Selectivity. *Nat. Commun.* **2021**, *12*, 17.
(35) Zhang, L.; Chen, K.; Chen, B.; White, J. L.; Resasco, D. E. Factors that Determine Zeolite Stability in Hot Liquid Water. *J. Am. Chem. Soc.* **2015**, *137*, 11810−11819.
(36) Aramburo, L. R.; Ruiz-Martínez, J.; Sommer, L.; Arstad, B.; Buitrago-Sierra, R.; Sepúlveda-Escribano, A.; Zandbergen, H. W.; Olsbye, U.; de Groot, F. M. F.; Weckhuysen, B. M. X-Ray Imaging of SAPO-34 Molecular Sieves at the Nanoscale: Influence of Steaming on the Methanol-to-Hydrocarbons Reaction. *ChemCatChem.* **2013**, *5*, 1386−1394.
(37) Bregante, D. T.; Chan, M. C.; Tan, J. Z.; Ayla, E. Z.; Nicholas, C. P.; Shukla, D.; Flaherty, D. W. The Shape of Water in Zeolites and Its Impact on Epoxidation Catalysis. *Nat. Catal.* **2021**, *4*, 797−808.
(38) Hack, J. H.; Dombrowski, J. P.; Ma, X.; Chen, Y.; Lewis, N. H. C.; Carpenter, W. B.; Li, C.; Voth, G. A.; Kung, H. H.; Tokmakoff, A. Structural Characterization of Protonated Water Clusters Confined in HZSM-5 Zeolites. *J. Am. Chem. Soc.* **2021**, *143*, 10203−10213.
(39) Kuo, I.-F. W.; Mundy, C. J. An ab Initio Molecular Dynamics Study of the Aqueous Liquid-Vapor Interface. *Science* **2004**, *303*, 658−660.
(40) Headrick, J. M.; Diken, E. G.; Walters, R. S.; Hammer, N. I.; Christie, R. A.; Cui, J.; Myshakin, E. M.; Duncan, M. A.; Johnson, M. A.; Jordan, K. D. Spectral Signatures of Hydrated Proton Vibrations in Water Clusters. *Science* **2005**, *308*, 1765−1769.
(41) Shin, J. W.; Hammer, N. I.; Diken, E. G.; Johnson, M. A.; Walters, R. S.; Jaeger, T. D.; Duncan, M. A.; Christie, R. A.; Jordan, K. D. Infrared Signature of Structures Associated with the $H^+(H_2O)_n$ (n = 6 to 27) Clusters. *Science* **2004**, *304*, 1137−1140.
(42) Heard, C. J.; Grajciar, L.; Nachtigall, P. The Effect of Water on the Validity of Lowenstein's Rule. *Chem. Sci.* **2019**, *10*, 5705−5711.
(43) Santoro, M.; Veremeienko, V.; Polisi, M.; Fantini, R.; Alabarse, F.; Arletti, R.; Quatieri, S.; Svitlyk, V.; van der Lee, A.; Rouquette, J.; Alonso, B.; Di Renzo, F.; Coasne, B.; Haines, J. Insertion and Confinement of H_2O in Hydrophobic Siliceous Zeolites at High Pressure. *J. Phys. Chem. C* **2019**, *123*, 17432−17439.
(44) Ashbrook, S. E.; Davis, Z. H.; Morris, R. E.; Rice, C. M. ^{17}O NMR Spectroscopy of Crystalline Microporous Materials. *Chem. Sci.* **2021**, *12*, 5016−5036.
(45) Huhn, C.; Erlebach, A.; Mey, D.; Wondraczek, L.; Sierka, M. Ab Initio Energetics of Si-O Bond Cleavage. *J. Comput. Chem.* **2017**, *38*, 2349−2353.
(46) Cypryk, M.; Apeloig, Y. Mechanism of the Acid-Catalyzed Si-O Bond Cleavage in Siloxanes and Siloxanols. A Theoretical Study. *Organometallics* **2002**, *21*, 2165−2175.
(47) Sun, J.; Fang, H.; Ravikovitch, P. I.; Sholl, D. S. Understanding Dealumination Mechanisms in Protonic and Cationic Zeolites. *J. Phys. Chem. C* **2020**, *124*, 668−676.
(48) Sun, T.; Xu, S.; Xiao, D.; Liu, Z.; Li, G.; Zheng, A.; Liu, W.; Xu, Z.; Cao, Y.; Guo, Q.; Wang, N.; Wei, Y.; Liu, Z. Water-Induced Structural Dynamic Process in Molecular Sieves under Mild Hydrothermal Conditions: Ship-in-a-Bottle Strategy for Acidity Identification and Catalyst Modification. *Angew. Chem., Int. Ed.* **2020**, *59*, 20672−20681.
(49) Yang, L.; Wang, C.; Zhang, L.; Dai, W.; Chu, Y.; Xu, J.; Wu, G.; Gao, M.; Liu, W.; Xu, Z.; Wang, P.; Guan, N.; Dyballa, M.; Ye, M.; Deng, F.; Fan, W.; Li, L. Stabilizing the Framework of SAPO-34 Zeolite toward Long-term Methanol-to-olefins Conversion. *Nat. Commun.* **2021**, *12*, 4661.
(50) Li, G.; Foo, C.; Yi, X.; Chen, W.; Zhao, P.; Gao, P.; Yoskamtorn, T.; Xiao, Y.; Day, S.; Tang, C. C.; Hou, G.; Zheng, A.; Tsang, S. C. E. Induced Active Sites by Adsorbate in Zeotype Materials. *J. Am. Chem. Soc.* **2021**, *143*, 8761−8771.
(51) Chen, W.; Han, J.; Wei, Y.; Zheng, A. Frustrated Lewis Pair in Zeolite Cages for Alkane Activations. *Angew. Chem., Int. Ed.* **2022**, DOI: 10.1002/anie.202116269.
(52) Bellussi, G.; Carati, A.; Clerici, M. G.; Maddinelli, G.; Millini, R. Reaction of Titanium Silicalite with Protic Molecules and Hydrogen Peroxide. *J. Catal.* **1992**, *133*, 220−230.
(53) Notari, B. Titanium Silicalites. *Catal. Today* **1993**, *18*, 163−172.
(54) To, J.; Sokol, A. A.; French, S. A.; Catlow, C. R. A. Formation of Active Sites in TS-1 by Hydrolysis and Inversion. *J. Phys. Chem. C* **2007**, *111*, 14720−14731.
(55) Qi, G.; Wang, Q.; Xu, J.; Wu, Q.; Wang, C.; Zhao, X.; Meng, X.; Xiao, F.; Deng, F. Direct Observation of Tin Sites and Their Reversible Interconversion in Zeolites by Solid-state NMR Spectroscopy. *Commun. Chem.* **2018**, *1*, 22.
(56) Ravi, M.; Sushkevich, V. L.; van Bokhoven, J. A. Towards a Better Understanding of Lewis Acidic Aluminium in Zeolites. *Nat. Mater.* **2020**, *19*, 1047−1056.
(57) Stanciakova, K.; Weckhuysen, B. M. Water−active Site Interactions in Zeolites and Their Relevance in Catalysis. *Trends Chem.* **2021**, *3*, 456−468.
(58) Resasco, D. E.; Crossley, S. P.; Wang, B.; White, J. L. Interaction of Water with Zeolites: A Review. *Catal. Rev.* **2021**, *63*, 302−362.
(59) Ravenelle, R. M.; Schüßler, F.; D'Amico, A.; Danilina, N.; van Bokhoven, J. A.; Lercher, J. A.; Jones, C. W.; Sievers, C. Stability of Zeolites in Hot Liquid Water. *J. Phys. Chem. C* **2010**, *114*, 19582−19595.
(60) Zhai, D.; Zhao, L.; Liu, Y.; Xu, J.; Shen, B.; Gao, J. Dissolution and Absorption: A Molecular Mechanism of Mesopore Formation in Alkaline Treatment of Zeolite. *Chem. Mater.* **2015**, *27*, 67−74.
(61) Malola, S.; Svelle, S.; Bleken, F. L.; Swang, O. Detailed Reaction Paths for Zeolite Dealumination and Desilication from Density Functional Calculations. *Angew. Chem., Int. Ed.* **2012**, *51*, 652−655.
(62) Nielsen, M.; Brogaard, R. Y.; Falsig, H.; Beato, P.; Swang, O.; Svelle, S. Kinetics of Zeolite Dealumination: Insights from H-SSZ-13. *ACS Catal.* **2015**, *5*, 7131−7139.
(63) Silaghi, M.-C.; Chizallet, C.; Petracovschi, E.; Kerber, T.; Sauer, J.; Raybaud, P. Regioselectivity of Al−O Bond Hydrolysis during Zeolites Dealumination Unified by Brønsted−Evans−Polanyi Relationship. *ACS Catal.* **2015**, *5*, 11−15.
(64) Silaghi, M.-C.; Chizallet, C.; Sauer, J.; Raybaud, P. Dealumination Mechanisms of Zeolites and Extra-framework Aluminum Confinement. *J. Catal.* **2016**, *339*, 242−255.
(65) Liu, P.; Liu, Q.; Mei, D. Dealumination of the H-BEA Zeolite via the S_{N2} Mechanism: A Theoretical Investigation. *J. Phys. Chem. C* **2021**, *125*, 24613−24621.
(66) Chen, K.; Horstmeier, S.; Nguyen, V. T.; Wang, B.; Crossley, S. P.; Pham, T.; Gan, Z.; Hung, I.; White, J. L. Structure and Catalytic Characterization of a Second Framework Al(IV) Site in Zeolite Catalysts Revealed by NMR at 35.2 T. *J. Am. Chem. Soc.* **2020**, *142*, 7514−7523.
(67) Chen, K.; Gan, Z.; Horstmeier, S.; White, J. L. Distribution of Aluminum Species in Zeolite Catalysts: ^{27}Al NMR of Framework, Partially-Coordinated Framework, and Non-Framework Moieties. *J. Am. Chem. Soc.* **2021**, *143*, 6669−6680.
(68) Stanciakova, K.; Ensing, B.; Göltl, F.; Bulo, R. E.; Weckhuysen, B. M. Cooperative Role of Water Molecules during the Initial Stage of Water-Induced Zeolite Dealumination. *ACS Catal.* **2019**, *9*, 5119−5135.
(69) Nielsen, M.; Hafreager, A.; Brogaard, R. Y.; De Wispelaere, K.; Falsig, H.; Beato, P.; Van Speybroeck, V.; Svelle, S. Collective Action of Water Molecules in Zeolite Dealumination. *Catal. Sci. Technol.* **2019**, *9*, 3721−3725.
(70) Zhou, T.; Bai, P.; Siepmann, J. I.; Clark, A. E. Deconstructing the Confinement Effect upon the Organization and Dynamics of Water in Hydrophobic Nanoporous Materials: Lessons Learned from Zeolites. *J. Phys. Chem. C* **2017**, *121*, 22015−22024.
(71) Qin, Z.; Zeng, S.; Melinte, G.; Bucko, T.; Badawi, M.; Shen, Y.; Gilson, J. P.; Ersen, O.; Wei, Y.; Liu, Z.; Liu, X.; Yan, Z.; Xu, S.; Valtchev, V.; Mintova, S. Understanding the Fundamentals of

Microporosity Upgrading in Zeolites: Increasing Diffusion and Catalytic Performances. *Adv. Sci.* **2021**, *8*, No. 2100001.
(72) Smith, L.; Cheetham, A. K.; Morris, R. E.; Marchese, L.; Thomas, J. M.; Wright, P. A.; Chen, J. On the Nature of Water Bound to a Solid Acid Catalyst. *Science* **1996**, *271*, 799−802.
(73) Termath, V.; Haase, F.; Sauer, J.; Hutter, J.; Parrinello, M. Understanding the Nature of Water Bound to Solid Acid Surfaces. Ab Initio Simulation on HSAPO-34. *J. Am. Chem. Soc.* **1998**, *120*, 8512−8516.
(74) Fjermestad, T.; Svelle, S.; Swang, O. Mechanistic Comparison of the Dealumination in SSZ-13 and the Desilication in SAPO-34. *J. Phys. Chem. C* **2013**, *117*, 13442−13451.
(75) Fjermestad, T.; Svelle, S.; Swang, O. Desilication of SAPO-34: Reaction Mechanisms from Periodic DFT Calculations. *J. Phys. Chem. C* **2015**, *119*, 2073−2085.
(76) Fjermestad, T.; Svelle, S.; Swang, O. Mechanism of Si Island Formation in SAPO-34. *J. Phys. Chem. C* **2015**, *119*, 2086−2095.
(77) Kalantzopoulos, G. N.; Lundvall, F.; Thorshaug, K.; Lind, A.; Vajeeston, P.; Dovgaliuk, I.; Arstad, B.; Wragg, D. S.; Fjellvåg, H. Factors Determining Microporous Material Stability in Water: The Curious Case of SAPO-37. *Chem. Mater.* **2020**, *32*, 1495−1505.
(78) Ferrini, P.; Dijkmans, J.; De Clercq, R.; Van de Vyver, S.; Dusselier, M.; Jacobs, P. A.; Sels, B. F. Lewis Acid Catalysis on Single Site Sn Centers Incorporated into Silica Hosts. *Coord. Chem. Rev.* **2017**, *343*, 220−255.
(79) Wolf, P.; Valla, M.; Núñez-Zarur, F.; Comas-Vives, A.; Rossini, A. J.; Firth, C.; Kallas, H.; Lesage, A.; Emsley, L.; Copéret, C.; Hermans, I. Correlating Synthetic Methods, Morphology, Atomic-Level Structure, and Catalytic Activity of Sn-β Catalysts. *ACS Catal.* **2016**, *6*, 4047−4063.
(80) Sushkevich, V. L.; Kots, P. A.; Kolyagin, Y. G.; Yakimov, A. V.; Marikutsa, A. V.; Ivanova, I. I. Origin of Water-Induced Brønsted Acid Sites in Sn-BEA Zeolites. *J. Phys. Chem. C* **2019**, *123*, 5540−5548.
(81) Yakimov, A. V.; Kolyagin, Y. G.; Tolborg, S.; Vennestrøm, P. N. R.; Ivanova, I. I. ^{119}Sn MAS NMR Study of the Interaction of Probe Molecules with Sn-BEA: The Origin of Penta- and Hexacoordinated Tin Formation. *J. Phys. Chem. C* **2016**, *120*, 28083−28092.
(82) Jin, M.; Veselý, O.; Heard, C. J.; Kubů, M.; Nachtigall, P.; Čejka, J.; Grajciar, L. The Role of Water Loading and Germanium Content in Germanosilicate Hydrolysis. *J. Phys. Chem. C* **2021**, *125*, 23744−23757.
(83) Del Campo, P.; Martinez, C.; Corma, A. Activation and Conversion of Alkanes in the Confined Space of Zeolite-type Materials. *Chem. Soc. Rev.* **2021**, *50*, 8511−8595.
(84) Snyder, B. E. R.; Bols, M. L.; Schoonheydt, R. A.; Sels, B. F.; Solomon, E. I. Iron and Copper Active Sites in Zeolites and Their Correlation to Metalloenzymes. *Chem. Rev.* **2018**, *118*, 2718−2768.
(85) Kiani, D.; Sourav, S.; Tang, Y.; Baltrusaitis, J.; Wachs, I. E. Methane Activation by ZSM-5-supported Transition Metal Centers. *Chem. Soc. Rev.* **2021**, *50*, 1251−1268.
(86) Paolucci, C.; Di Iorio, J. R.; Schneider, W. F.; Gounder, R. Solvation and Mobilization of Copper Active Sites in Zeolites by Ammonia: Consequences for the Catalytic Reduction of Nitrogen Oxides. *Acc. Chem. Res.* **2020**, *53*, 1881−1892.
(87) Borfecchia, E.; Beato, P.; Svelle, S.; Olsbye, U.; Lamberti, C.; Bordiga, S. Cu-CHA - a Model System for Applied Selective Redox Catalysis. *Chem. Soc. Rev.* **2018**, *47*, 8097−8133.
(88) Tomkins, P.; Ranocchiari, M.; van Bokhoven, J. A. Direct Conversion of Methane to Methanol under Mild Conditions over Cu-Zeolites and beyond. *Acc. Chem. Res.* **2017**, *50*, 418−425.
(89) Ravi, M.; Sushkevich, V. L.; Knorpp, A. J.; Newton, M. A.; Palagin, D.; Pinar, A. B.; Ranocchiari, M.; van Bokhoven, J. A. Misconceptions and Challenges in Methane-to-methanol over Transition-metal-exchanged Zeolites. *Nat. Catal.* **2019**, *2*, 485−494.
(90) Newton, M. A.; Knorpp, A. J.; Sushkevich, V. L.; Palagin, D.; van Bokhoven, J. A. Active Sites and Mechanisms in the Direct Conversion of Methane to Methanol using Cu in Zeolitic Hosts: A Critical Examination. *Chem. Soc. Rev.* **2020**, *49*, 1449−1486.
(91) Freakley, S. J.; Dimitratos, N.; Willock, D. J.; Taylor, S. H.; Kiely, C. J.; Hutchings, G. J. Methane Oxidation to Methanol in Water. *Acc. Chem. Res.* **2021**, *54*, 2614−2623.
(92) Snyder, B. E.; Vanelderen, P.; Bols, M. L.; Hallaert, S. D.; Bottger, L. H.; Ungur, L.; Pierloot, K.; Schoonheydt, R. A.; Sels, B. F.; Solomon, E. I. The Active Site of Low-temperature Methane Hydroxylation in Iron-containing Zeolites. *Nature* **2016**, *536*, 317−321.
(93) Bols, M. L.; Snyder, B. E. R.; Rhoda, H. M.; Cnudde, P.; Fayad, G.; Schoonheydt, R. A.; Van Speybroeck, V.; Solomon, E. I.; Sels, B. F. Coordination and Activation of Nitrous Oxide by Iron Zeolites. *Nat. Catal.* **2021**, *4* (4), 332−340.
(94) Snyder, B. E. R.; Bols, M. L.; Rhoda, H. M.; Plessers, D.; Schoonheydt, R. A.; Sels, B. F.; Solomon, E. I. Cage Effects Control the Mechanism of Methane Hydroxylation in Zeolites. *Science* **2021**, *373*, 327−331.
(95) Scott, S. L. Bioinspired Methane Oxidation in a Zeolite. *Science* **2021**, *373*, 277−278.
(96) Li, G.; Pidko, E. A.; van Santen, R. A.; Li, C.; Hensen, E. J. M. Stability of Extraframework Iron-Containing Complexes in ZSM-5 Zeolite. *J. Phys. Chem. C* **2013**, *117*, 413−426.
(97) Szecsenyi, A.; Li, G.; Gascon, J.; Pidko, E. A. Mechanistic Complexity of Methane Oxidation with H_2O_2 by Single-Site Fe/ZSM-5 Catalyst. *ACS Catal.* **2018**, *8*, 7961−7972.
(98) Szécsényi, Á.; Khramenkova, E.; Chernyshov, I. Y.; Li, G.; Gascon, J.; Pidko, E. A. Breaking Linear Scaling Relationships with Secondary Interactions in Confined Space: A Case Study of Methane Oxidation by Fe/ZSM-5 Zeolite. *ACS Catal.* **2019**, *9*, 9276−9284.
(99) Li, G.; Pidko, E. A.; Filot, I. A. W.; van Santen, R. A.; Li, C.; Hensen, E. J. M. Catalytic Properties of Extraframework Iron-containing Species in ZSM-5 for N_2O Decomposition. *J. Catal.* **2013**, *308*, 386−397.
(100) Negri, C.; Signorile, M.; Porcaro, N. G.; Borfecchia, E.; Berlier, G.; Janssens, T. V. W.; Bordiga, S. Dynamic Cu^{II}/Cu^{I} Speciation in Cu-CHA Catalysts by in situ Diffuse Reflectance UV−vis-NIR Spectroscopy. *Appl. Catal., A* **2019**, *578*, 1−9.
(101) Li, H.; Paolucci, C.; Khurana, I.; Wilcox, L. N.; Goltl, F.; Albarracin-Caballero, J. D.; Shih, A. J.; Ribeiro, F. H.; Gounder, R.; Schneider, W. F. Consequences of Exchange-site Heterogeneity and Dynamics on the UV-visible Spectrum of Cu-Exchanged SSZ-13. *Chem. Sci.* **2019**, *10*, 2373−2384.
(102) Chen, P.; Khetan, A.; Jabłońska, M.; Simböck, J.; Muhler, M.; Palkovits, R.; Pitsch, H.; Simon, U. Local Dynamics of Copper Active Sites in Zeolite Catalysts for Selective Catalytic Reduction of NO_x with NH_3. *Appl. Catal., B* **2018**, *237*, 263−272.
(103) Seiyama, T.; Arakawa, T.; Matsuda, T.; Takita, Y.; Yamazoe, N. Catalytic Activity of Transition Metal Ion Exchanged Y Zeolites in the Reduction of Nitric Oxide with Ammonia. *J. Catal.* **1977**, *48*, 1−7.
(104) Negri, C.; Selleri, T.; Borfecchia, E.; Martini, A.; Lomachenko, K. A.; Janssens, T. V. W.; Cutini, M.; Bordiga, S.; Berlier, G. Structure and Reactivity of Oxygen-Bridged Diamino Dicopper(II) Complexes in Cu-Ion-Exchanged Chabazite Catalyst for NH_3-Mediated Selective Catalytic Reduction. *J. Am. Chem. Soc.* **2020**, *142*, 15884−15896.
(105) Paolucci, C.; Parekh, A. A.; Khurana, I.; Di Iorio, J. R.; Li, H.; Albarracin Caballero, J. D.; Shih, A. J.; Anggara, T.; Delgass, W. N.; Miller, J. T.; Ribeiro, F. H.; Gounder, R.; Schneider, W. F. Catalysis in a Cage: Condition-Dependent Speciation and Dynamics of Exchanged Cu Cations in SSZ-13 Zeolites. *J. Am. Chem. Soc.* **2016**, *138*, 6028−6048.
(106) Gramigni, F.; Nasello, N. D.; Usberti, N.; Iacobone, U.; Selleri, T.; Hu, W.; Liu, S.; Gao, X.; Nova, I.; Tronconi, E. Transient Kinetic Analysis of Low-Temperature NH_3-SCR over Cu-CHA Catalysts Reveals a Quadratic Dependence of Cu Reduction Rates on Cu^{II}. *ACS Catal.* **2021**, *11*, 4821−4831.
(107) Paolucci, C.; Khurana, I.; Parekh, A. A.; Li, S.; Shih, A. J.; Li, H.; Di Iorio, J. R.; Albarracin-Caballero, J. D.; Yezerets, A.; Miller, J. T.; Delgass, W. N.; Ribeiro, F. H.; Schneider, W. F.; Gounder, R. Dynamic Multinuclear Sites formed by Mobilized Copper Ions in NO_x Selective Catalytic Reduction. *Science* **2017**, *357*, 898−903.

https://doi.org/10.1021/acscatal.2c01233
ACS Catal. 2022, 12, 5060−5076

(108) Sushkevich, V. L.; Palagin, D.; Ranocchiari, M.; van Bokhoven, J. A. Selective Anaerobic Oxidation of Methane Enables Direct Synthesis of Methanol. *Science* **2017**, *356*, 523−527.
(109) Xu, R.; Liu, N.; Dai, C.; Li, Y.; Zhang, J.; Wu, B.; Yu, G.; Chen, B. H_2O-Built Proton Transfer Bridge Enhances Continuous Methane Oxidation to Methanol over Cu-BEA Zeolite. *Angew. Chem., Int. Ed.* **2021**, *60*, 16634−16640.
(110) Engedahl, U.; Grönbeck, H.; Hellman, A. First-Principles Study of Oxidation State and Coordination of Cu-Dimers in Cu-SSZ-13 during Methane-to-Methanol Reaction Conditions. *J. Phys. Chem. C* **2019**, *123*, 26145−26150.
(111) Göltl, F.; Bhandari, S.; Mavrikakis, M. Thermodynamics Perspective on the Stepwise Conversion of Methane to Methanol over Cu-Exchanged SSZ-13. *ACS Catal.* **2021**, *11*, 7719−7734.
(112) Sun, L.; Wang, Y.; Wang, C.; Xie, Z.; Guan, N.; Li, L. Water-involved Methane-selective Catalytic Oxidation by Dioxygen over Copper Zeolites. *Chem* **2021**, *7*, 1557−1568.
(113) Pan, X.; Jiao, F.; Miao, D.; Bao, X. Oxide-Zeolite-Based Composite Catalyst Concept That Enables Syngas Chemistry beyond Fischer−Tropsch Synthesis. *Chem. Rev.* **2021**, *121*, 6588−6609.
(114) Gao, J.; Zheng, Y.; Jehng, J.-M.; Tang, Y.; Wachs, I. E.; Podkolzin, S. G. Identification of Molybdenum Oxide Nanostructures on Zeolites for Natural Gas Conversion. *Science* **2015**, *348*, 686−690.
(115) Vollmer, I.; van der Linden, B.; Ould-Chikh, S.; Aguilar-Tapia, A.; Yarulina, I.; Abou-Hamad, E.; Sneider, Y. G.; Olivos Suarez, A. I.; Hazemann, J. L.; Kapteijn, F.; Gascon, J. On the Dynamic Nature of Mo Sites for Methane Dehydroaromatization. *Chem. Sci.* **2018**, *9*, 4801−4807.
(116) Tempelman, C. H. L.; Hensen, E. J. M. On the Deactivation of Mo/HZSM-5 in the Methane Dehydroaromatization Reaction. *Appl. Catal., B* **2015**, *176*−*177*, 731−739.
(117) Han, S. J.; Kim, S. K.; Hwang, A.; Kim, S.; Hong, D.-Y.; Kwak, G.; Jun, K.-W.; Kim, Y. T. Non-oxidative Dehydroaromatization of Methane over Mo/H-ZSM-5 Catalysts: A Detailed Analysis of the Reaction-regeneration Cycle. *Appl. Catal., B* **2019**, *241*, 305−318.
(118) Lezcano-González, I.; Oord, R.; Rovezzi, M.; Glatzel, P.; Botchway, S. W.; Weckhuysen, B. M.; Beale, A. M. Molybdenum Speciation and its Impact on Catalytic Activity during Methane Dehydroaromatization in Zeolite ZSM-5 as Revealed by Operando X-Ray Methods. *Angew. Chem., Int. Ed.* **2016**, *55*, 5215−5219.
(119) Vollmer, I.; Kosinov, N.; Szécsényi, Á.; Li, G.; Yarulina, I.; Abou-Hamad, E.; Gurinov, A.; Ould-Chikh, S.; Aguilar-Tapia, A.; Hazemann, J.-L.; Pidko, E.; Hensen, E.; Kapteijn, F.; Gascon, J. A Site-sensitive *quasi-in situ* Strategy to Characterize Mo/HZSM-5 during Activation. *J. Catal.* **2019**, *370*, 321−331.
(120) Zheng, Y.; Tang, Y.; Gallagher, J. R.; Gao, J.; Miller, J. T.; Wachs, I. E.; Podkolzin, S. G. Molybdenum Oxide, Oxycarbide, and Carbide: Controlling the Dynamic Composition, Size, and Catalytic Activity of Zeolite-Supported Nanostructures. *J. Phys. Chem. C* **2019**, *123*, 22281−22292.
(121) Kosinov, N.; Wijpkema, A. S. G.; Uslamin, E.; Rohling, R.; Coumans, F.; Mezari, B.; Parastaev, A.; Poryvaev, A. S.; Fedin, M. V.; Pidko, E. A.; Hensen, E. J. M. Confined Carbon Mediating Dehydroaromatization of Methane over Mo/ZSM-5. *Angew. Chem., Int. Ed.* **2018**, *57*, 1016−1020.
(122) Kosinov, N.; Coumans, F. J. A. G.; Li, G.; Uslamin, E.; Mezari, B.; Wijpkema, A. S. G.; Pidko, E. A.; Hensen, E. J. M. Stable Mo/HZSM-5 Methane Dehydroaromatization Catalysts Optimized for High-temperature Calcination-regeneration. *J. Catal.* **2017**, *346*, 125−133.
(123) Vollmer, I.; Ould-Chikh, S.; Aguilar-Tapia, A.; Li, G.; Pidko, E.; Hazemann, J. L.; Kapteijn, F.; Gascon, J. Activity Descriptors Derived from Comparison of Mo and Fe as Active Metal for Methane Conversion to Aromatics. *J. Am. Chem. Soc.* **2019**, *141*, 18814−18824.
(124) Wang, L.-C.; Zhang, Y.; Xu, J.; Diao, W.; Karakalos, S.; Liu, B.; Song, X.; Wu, W.; He, T.; Ding, D. Non-oxidative Dehydrogenation of Ethane to Ethylene over ZSM-5 Zeolite Supported Iron Catalysts. *Appl. Catal., B* **2019**, *256*, 117816.
(125) Gu, Y.; Chen, P.; Wang, X.; Lyu, Y.; Liu, W.; Liu, X.; Yan, Z. Active Sites and Induction Period of Fe/ZSM-5 Catalyst in Methane Dehydroaromatization. *ACS Catal.* **2021**, *11*, 6771−6786.
(126) Copéret, C.; Estes, D. P.; Larmier, K.; Searles, K. Isolated Surface Hydrides: Formation, Structure, and Reactivity. *Chem. Rev.* **2016**, *116*, 8463−8505.
(127) Vidal, V.; Théolier, A.; Thivolle-Cazat, J.; Basset, J.-M. Metathesis of Alkanes Catalyzed by Silica-Supported Transition Metal Hydrides. *Science* **1997**, *276*, 99−102.
(128) Zhou, Y.; Thirumalai, H.; Smith, S. K.; Whitmire, K. H.; Liu, J.; Frenkel, A. I.; Grabow, L. C.; Rimer, J. D. Ethylene Dehydroaromatization over Ga-ZSM-5 Catalysts: Nature and Role of Gallium Speciation. *Angew. Chem., Int. Ed.* **2020**, *59*, 19592−19601.
(129) Kazansky, V. B.; Subbotina, I. R.; van Santen, R. A.; Hensen, E. J. M. DRIFTS Study of the Chemical State of Modifying Gallium Ions in Reduced Ga/ZSM-5 Prepared by ImpregnationI. Observation of Gallium Hydrides and Application of CO Adsorption as a Molecular Probe for Reduced Gallium Ions. *J. Catal.* **2004**, *227*, 263−269.
(130) Kazansky, V.; Subbotina, I.; Vansanten, R.; Hensen, E. DRIFTS Study of the Nature and Chemical Reactivity of Gallium Ions in Ga/ZSM-5 II. Oxidation of Reduced Ga Species in ZSM-5 by Nitrous Oxide or Water. *J. Catal.* **2005**, *233*, 351−358.
(131) Schreiber, M. W.; Plaisance, C. P.; Baumgartl, M.; Reuter, K.; Jentys, A.; Bermejo-Deval, R.; Lercher, J. A. Lewis-Brønsted Acid Pairs in Ga/H-ZSM-5 to Catalyze Dehydrogenation of Light Alkanes. *J. Am. Chem. Soc.* **2018**, *140*, 4849−4859.
(132) Mansoor, E.; Head-Gordon, M.; Bell, A. T. Computational Modeling of the Nature and Role of Ga Species for Light Alkane Dehydrogenation Catalyzed by Ga/H-MFI. *ACS Catal.* **2018**, *8*, 6146−6162.
(133) Phadke, N. M.; Van der Mynsbrugge, J.; Mansoor, E.; Getsoian, A. B.; Head-Gordon, M.; Bell, A. T. Characterization of Isolated Ga^{3+} Cations in Ga/H-MFI Prepared by Vapor-phase Exchange of H-MFI Zeolite with $GaCl_3$. *ACS Catal.* **2018**, *8*, 6106−6126.
(134) Phadke, N. M.; Mansoor, E.; Bondil, M.; Head-Gordon, M.; Bell, A. T. Mechanism and Kinetics of Propane Dehydrogenation and Cracking over Ga/H-MFI Prepared via Vapor-phase Exchange of H-MFI with $GaCl_3$. *J. Am. Chem. Soc.* **2019**, *141*, 1614−1627.
(135) Phadke, N. M.; Mansoor, E.; Head-Gordon, M.; Bell, A. T. Mechanism and Kinetics of Light Alkane Dehydrogenation and Cracking over Isolated Ga Species in Ga/H-MFI. *ACS Catal.* **2021**, *11*, 2062−2075.
(136) Raad, M.; Hamieh, S.; Toufaily, J.; Hamieh, T.; Pinard, L. Propane Aromatization on Hierarchical Ga/HZSM-5 Catalysts. *J. Catal.* **2018**, *366*, 223−236.
(137) Yuan, Y.; Brady, C.; Lobo, R. F.; Xu, B. Understanding the Correlation between Ga Speciation and Propane Dehydrogenation Activity on Ga/H-ZSM-5 Catalysts. *ACS Catal.* **2021**, *11*, 10647−10659.
(138) Maeno, Z.; Yasumura, S.; Wu, X.; Huang, M.; Liu, C.; Toyao, T.; Shimizu, K. I. Isolated Indium Hydrides in CHA Zeolites: Speciation and Catalysis for Nonoxidative Dehydrogenation of Ethane. *J. Am. Chem. Soc.* **2020**, *142*, 4820−4832.
(139) Kazansky, V. B.; Serykh, A. I. Unusual Localization of Zinc Cations in MFI Zeolites Modified by Different Ways of Preparation. *Phys. Chem. Chem. Phys.* **2004**, *6*, 3760−3764.
(140) Barbosa, L. A. M. M.; van Santen, R. A. The Activation of H_2 by Zeolitic Zn(II) Cations. *J. Phys. Chem. C* **2007**, *111*, 8337−8348.
(141) Oda, A.; Torigoe, H.; Itadani, A.; Ohkubo, T.; Yumura, T.; Kobayashi, H.; Kuroda, Y. Unprecedented Reversible Redox Process in the ZnMFI-H_2 System Involving Formation of Stable Atomic Zn^0. *Angew. Chem., Int. Ed.* **2012**, *51*, 7719−7723.
(142) Shimizu, K.-i.; Sugino, K.; Kato, K.; Yokota, S.; Okumura, K.; Satsuma, A. Formation and Redispersion of Silver Clusters in Ag-MFI Zeolite as Investigated by Time-Resolved QXAFS and UV-Vis. *J. Phys. Chem. C* **2007**, *111*, 1683−1688.

https://doi.org/10.1021/acscatal.2c01233
ACS Catal. 2022, 12, 5060−5076

(143) Okumura, K.; Kato, K.; Sanada, T.; Niwa, M. In-Situ QXAFS Studies on the Dynamic Coalescence and Dispersion Processes of Pd in the. *J. Phys. Chem. C* **2007**, *111*, 14426−14432.
(144) Okumura, K.; Honma, T.; Hirayama, S.; Sanada, T.; Niwa, M. Stepwise Growth of Pd Clusters in USY Zeolite at Room Temperature Analyzed by QXAFS. *J. Phys. Chem. C* **2008**, *112*, 16740−16747.
(145) Lardinois, T. M.; Bates, J. S.; Lippie, H. H.; Russell, C. K.; Miller, J. T.; Meyer, H. M.; Unocic, K. A.; Prikhodko, V.; Wei, X.; Lambert, C. K.; Getsoian, A. B.; Gounder, R. Structural Interconversion between Agglomerated Palladium Domains and Mononuclear Pd(II) Cations in Chabazite Zeolites. *Chem. Mater.* **2021**, *33*, 1698−1713.
(146) Moliner, M.; Gabay, J. E.; Kliewer, C. E.; Carr, R. T.; Guzman, J.; Casty, G. L.; Serna, P.; Corma, A. Reversible Transformation of Pt Nanoparticles into Single Atoms Inside High-silica Chabazite Zeolite. *J. Am. Chem. Soc.* **2016**, *138*, 15743−15750.
(147) Liu, L.; Zakharov, D. N.; Arenal, R.; Concepcion, P.; Stach, E. A.; Corma, A. Evolution and Stabilization of Subnanometric Metal Species in Confined Space by in situ TEM. *Nat. Commun.* **2018**, *9*, 574.
(148) Liu, L.; Lopez-Haro, M.; Lopes, C. W.; Meira, D. M.; Concepcion, P.; Calvino, J. J.; Corma, A. Atomic-level Understanding on the Evolution Behavior of Subnanometric Pt and Sn Species during High-temperature Treatments for Generation of Dense PtSn Clusters in Zeolites. *J. Catal.* **2020**, *391*, 11−24.
(149) Bukowski, B. C.; Delgass, W. N.; Greeley, J. Gold Stability and Diffusion in the Au/TS-1 Catalyst. *J. Phys. Chem. C* **2021**, *125*, 4519−4531.
(150) Wang, Y.; Wang, G.; van der Wal, L. I.; Cheng, K.; Zhang, Q.; de Jong, K. P.; Wang, Y. Visualizing Element Migration over Bifunctional Metal-Zeolite Catalysts and its Impact on Catalysis. *Angew. Chem., Int. Ed.* **2021**, *60*, 17735−17743.
(151) Agostini, G.; Lamberti, C.; Palin, L.; Milanesio, M.; Danilina, N.; Xu, B.; Janousch, M.; van Bokhoven, J. A. In Situ XAS and XRPD Parametric Rietveld Refinement To Understand Dealumination of Y Zeolite Catalyst. *J. Am. Chem. Soc.* **2010**, *132*, 667−678.
(152) Morris, S. A.; Bignami, G. P. M.; Tian, Y.; Navarro, M.; Firth, D. S.; Cejka, J.; Wheatley, P. S.; Dawson, D. M.; Slawinski, W. A.; Wragg, D. S.; Morris, R. E.; Ashbrook, S. E. In Situ Solid-state NMR and XRD Studies of the ADOR Process and the Unusual Structure of Zeolite IPC-6. *Nat. Chem.* **2017**, *9*, 1012−1018.
(153) Vjunov, A.; Fulton, J. L.; Huthwelker, T.; Pin, S.; Mei, D.; Schenter, G. K.; Govind, N.; Camaioni, D. M.; Hu, J. Z.; Lercher, J. A. Quantitatively Probing the Al Distribution in Zeolites. *J. Am. Chem. Soc.* **2014**, *136*, 8296−8306.
(154) van Bokhoven, J. A.; van der Eerden, A. M. J.; Koningsberger, D. C. Three-Coordinate Aluminum in Zeolites Observed with In situ X-ray Absorption Near-Edge Spectroscopy at the Al K-Edge: Flexibility of Aluminum Coordinations in Zeolites. *J. Am. Chem. Soc.* **2003**, *125*, 7435−7442.
(155) Vjunov, A.; Derewinski, M. A.; Fulton, J. L.; Camaioni, D. M.; Lercher, J. A. Impact of Zeolite Aging in Hot Liquid Water on Activity for Acid-Catalyzed Dehydration of Alcohols. *J. Am. Chem. Soc.* **2015**, *137*, 10374−10382.
(156) Harris, J. W.; Cordon, M. J.; Di Iorio, J. R.; Vega-Vila, J. C.; Ribeiro, F. H.; Gounder, R. Titration and Quantification of Open and Closed Lewis Acid Sites in Sn-Beta Zeolites that Catalyze Glucose Isomerization. *J. Catal.* **2016**, *335*, 141−154.
(157) Bordiga, S.; Lamberti, C.; Bonino, F.; Travert, A.; Thibault-Starzyk, F. Probing Zeolites by Vibrational Spectroscopies. *Chem. Soc. Rev.* **2015**, *44*, 7262−7341.
(158) Bruzzese, P. C.; Salvadori, E.; Jager, S.; Hartmann, M.; Civalleri, B.; Poppl, A.; Chiesa, M. ^{17}O-EPR Determination of the Structure and Dynamics of Copper Single-metal Sites in Zeolites. *Nat. Commun.* **2021**, *12*, 4638.
(159) Partridge, W. P.; Joshi, S. Y.; Pihl, J. A.; Currier, N. W. New Operando Method for Quantifying the Relative Half-cycle Rates of the NO SCR Redox Cycle over Cu-Exchanged Zeolites. *Appl. Catal., B* **2018**, *236*, 195−204.
(160) Daya, R.; Joshi, S. Y.; Luo, J.; Dadi, R. K.; Currier, N. W.; Yezerets, A. On Kinetic Modeling of Change in Active Sites upon Hydrothermal Aging of Cu-SSZ-13. *Appl. Catal., B* **2020**, *263*, 118368.

https://doi.org/10.1021/acscatal.2c01233
ACS Catal. 2022, 12, 5060−5076